Macroscopic model for unsteady generalized Newtonian fluid flow in homogeneous porous media

J. Sánchez-Vargas, F.J. Valdés-Parada, Didier Lasseux

Journal of Non-Newtonian Fluid Mechanics 306 (2022) 104840
https://doi.org/10.1016/j.jnnfm.2022.104840

Macroscopic model for unsteady generalized Newtonian fluid flow in homogeneous porous media

J. Sánchez-Vargas [a], F.J. Valdés-Parada [b], D. Lasseux [c]

[a] Departamento de Biología Molecular y Biotecnología, Instituto de Investigaciones Biomédicas, Universidad Nacional Autónoma de Mexico, CDMX, 04510, Mexico
[b] División de Ciencias Básicas e Ingeniería. Universidad Autónoma Metropolitana-Iztapalapa, Av. San Rafael Atlixco 186, col. Vicentina, CDMX, 09340, Mexico
[c] I2M, UMR 5295, CNRS, Univ. Bordeaux, 351 Cours de la Libération, 33405, Talence CEDEX, France

Keywords:
Porous media
Non-Newtonian flow
Volume averaging
Adjoint method
Green's formulas

A B S T R A C T

A macroscopic model for unsteady incompressible isothermal non-Newtonian flow in homogeneous porous media, taking into account inertial and slip effects at solid–fluid interfaces, is derived in this work. The development is carried out considering a general Newton's law of viscosity for the fluid phase. Using the classical volume averaging method, the seepage velocity is shown to be solenoidal. The macroscopic momentum equation is derived in the Laplace domain, employing a simplified version of the volume averaging method, which calls upon Green's formulas and adjoint problems for Green's function pairs for the velocity and pressure. In the Laplace domain, the macroscopic momentum equation takes the form of Darcy's law corrected by a term that accounts for the initial flow condition. Once transformed back into the time domain, this equation provides the macroscopic velocity that depends on two terms. The first one is under the form of a time convolution between the macroscopic pressure gradient and the time derivative of an apparent permeability tensor. The second one is a memory term that accounts for the effect of the initial flow conditions. These two effective quantities are determined from the solution of a single closure problem that naturally results from the derivations. The model is consistent with the unsteady model in the Newtonian case and simplifies to the steady versions of some non-Newtonian macroscopic flow models. The macroscopic model is validated with pore-scale simulations performed in 2D model porous structures, considering a Carreau fluid. The impact of inertia and non-Newtonian effects on the dynamics of the macroscopic coefficients is highlighted.

1. Introduction

Non-Newtonian fluid flow in porous media is of interest in many applications such as biological systems [1], food engineering [2], biomedical research [3], enhanced oil recovery (EOR) [4], as well as in the pharmaceutical, textile, polymer and composites industries [5], to list a few. Interest in this topic was strengthened after the formalization of viscous instability for two-phase flow in porous media [6], which contributed to intensify the use of aqueous species to increase water viscosity in EOR processes [7]. This made the study of non-Newtonian flow in porous media an important research topic in engineering during the second half of the 60's, as testified by the abundant literature on the subject during this period. Unfortunately, theoretical tools to derive macroscopic flow models in porous media were still at their infant stage at this time. First attempts to formally derive Darcy's law in the Newtonian case were published in the late 60's [8,9], but were completed years later [10–12]. This probably explains why one-phase macroscopic models for non-Newtonian flow in porous media widely remained empirical (see reviews in [13–15]) until the late 90's. The common practice in engineering applications has been to extend Darcy's law with an effective viscosity to that flow situation.

Nowadays, the study of porous media systems can be carried out by performing pore-scale simulations in detailed reconstructions of the porous matrix topology [16] or by developing upscaled models that capture the essential information from the microscale and carry it to the macroscale. In this regard, there are many upscaling techniques available as reviewed in [17]. However, the derivation of upscaled models for this type of flow is a challenging task due to the non-linear character that the momentum balance equation exhibits at the microscale, even under creeping flow conditions. Several upscaling approaches have been used to that purpose. For example, the macroscopic flux to force relationship has been inferred from simplified representations of the porous structure under the form of bundles of capillaries [18,19] and pore-network models [20,21]. More formal approaches have also been employed, including the thermodynamically

constrained averaging theory (TCAT) [22], the classical [23–37] and adjoint [38] homogenization techniques and the volume averaging method [39–42]. In the following paragraphs a brief literature review, mainly focused on applications of the homogenization and volume averaging methods, is presented. This is motivated by the fact that these upscaling approaches are those more closely related to the methodology used in this work, whereas an exhaustive literature review on the subject of non-Newtonian flow in porous media is beyond the scope of this paper.

The homogenization technique has been widely used to study non-Newtonian flow in porous media and a comprehensive overview on the subject is available from Mikelić [43]. The first attempts dealt with Bingham [23,24] and power-law and Carreau fluids under laminar flow conditions [25]. In the latter reference, Bourgeat and Mikelić reported that the auxiliary flow problem resulting from the power-series expansion is nonlinear but that it has, nevertheless, a unique solution that implicitly depends on the microstructure, the fluid properties and the macroscopic forcing. The micro- and macroscale coupling led Gipouloux and Zine [44] to use iterative algorithms to numerically solve the microscale and macroscale models in both isotropic and anisotropic geometries in the creeping regime. For the particular case of power-law fluids, Auriault et al. [27] concluded that the upscaled model can be expressed as an explicit nonlinear function of the macroscopic pressure gradient and an apparent permeability tensor that solely depends on the fluid properties only for transversely isotropic and orthotropic systems. These conclusions were later verified by Idris et al. [29] in other geometries.

The strong coupling issue between the pore-scale and the macroscale was addressed by Bourgeat et al. [28]. For a power-law fluid in particular, they showed, by means of numerical experiments, that the heuristic model commonly found in engineering is inappropriate , in general. For this reason, Fratrović and Marušić-Paloka [33] suggested to use the Darcy-like equation for a power-law model with the apparent permeability being the average of the solution of a quasi-Newtonian auxiliary problem. The same approach was used in other works to study non-Newtonian and quasi-steady flow through thin [34,35] and fractured [36,37] porous media. Götz and Parhusip [30] analyzed power-law and Carreau models under steady and creeping flow conditions. They were able to derive a closed model in the former case, whereas, in the latter, their procedure was restricted to flows that weakly depart from a Newtonian behavior. In that case, their closure procedure resulted from a second power series expansion with respect to the relaxation time parameter, yielding linear auxiliary closure problems. After performing comparisons with pore-scale simulations, they reported maximum errors of 5% for isotropic and 10% in anisotropic geometries. More recently, formal nonlinear solutions have been proposed for the flow problem corresponding to the zeroth-order power-series expansion [45,46], enabling the numerical solution of the problem in a periodic unit cell. Predictions of the pressure, velocity and viscosity were given through numerical simulations, however no validation was reported.

Using the adjoint homogenization approach [47], Airiau and Bottaro [38] considered the steady creeping flow of a shear-thinning incompressible fluid in the bulk of a porous medium. They proposed to first solve for the zeroth-order velocity in the power-series expansion and then substitute this field into the viscosity term of the auxiliary problem in order to avoid an iterative scheme. This also allowed them to readily derive a Darcy-type model, with the apparent permeability being an intrinsic function of the microstructure, the macroscopic forcing and the fluid properties. The philosophy of this work is continued here, albeit using a different upscaling approach and considering a more complicated flow problem as detailed in the next sections.

Regarding applications of the volume averaging method, fewer works have been reported in the literature. Liu and Masliyah [39] postulated a macroscale model for unsteady and inertial flow that resembles the Navier–Stokes equations in which a Darcy term, a tortuosity factor and a macroscopic viscosity are involved. Following more closely the classical volume averaging method [48], Tsakiroglou [40] derived a non-local and nonlinear closure problem and postulated that it should have a linear solution in terms of the average velocity. A similar approach was later reported by Wang et al. [41] for a power-law viscosity model in the creeping flow regime. Predictive capabilities of the proposed macroscopic model compared to numerical simulations and laboratory experiments were only qualitative. In essence, this supports the conclusion made by Zami-Pierre et al. [42] (see Appendix B therein), that the classical volume averaging approach cannot be used to derive closed models for non-Newtonian flow in porous media, even in the absence of inertia.

In most of the above mentioned derivations of upscaled models for non-Newtonian flow in porous media, steady-state conditions were assumed. Unsteadiness has been treated on an empirical basis, following the heuristic approach employed for Newtonian flow. It consists in modifying the empirical Darcy's law extended to the non-Newtonian case by the introduction of an accumulation term on the seepage velocity, as a replicate of the time acceleration term in the Navier–Stokes equation at the underlying pore-scale (see for instance [13,49,50]). However, such heuristic approach has been shown to be, in general, inadequate to model the seepage velocity dynamics in porous media [51,52]. A formal derivation in that case is therefore still lacking.

The purpose of this work is to reconsider the upscaling of non-Newtonian one-phase flow in homogeneous porous media in order to derive the macroscopic mass and momentum balance equations valid in the bulk of the medium (*i.e.*, far enough from the macroscopic boundaries) for unsteady, incompressible, laminar flow conditions, considering slip at the solid–fluid interface. This is done by using a modified version of the classical volume averaging method that is briefer as it benefits from elements of the adjoint homogenization method. This simplified volume averaging approach relies on the formulation and formal solution of the flow problem in a unit cell of the porous medium, the system being conceived as a periodic one, as routinely done with the homogenization approach (see, for instance [53]). This methodology has been successfully applied recently to study unsteady Newtonian flow in porous media under laminar and no-slip [51] as well as slip conditions [52]. The non-linearity introduced by the rheology represents a difficulty which, together with the slip effect, make it impossible to infer the corresponding macroscopic flow model from the derivation reported in these references, hence motivating the specific analysis proposed here.

The work is organized as follows. In Section 2, the governing equations at the pore scale are provided, together with the associated supporting assumptions. In Section 3, the essential elements to carry out the upscaling process using the volume averaging method and some elements of the adjoint technique are summarized. More specifically, the main definitions, theorems and expressions of Green's formulas are provided. These tools are employed in Section 4 to derive the corresponding macroscopic model for mass and momentum balance. The resulting macroscale model and its main features are summarized in Section 5. Section 6 is dedicated to the illustration of the model performance with some results obtained from numerical simulations carried out in a 2D model porous structure. First, predictions of the effective medium quantities involved in the macroscale momentum transport equation are reported and discussed. In a second step, the dynamics of the seepage velocity predicted by the macroscopic model is validated with pore-scale simulations. Finally, the corresponding conclusions are presented in Section 7.

2. Pore-scale model

Consider the single phase flow of a non-Newtonian fluid (*i.e.*, the β-phase) through the void space of a rigid and homogeneous porous medium (in the following the solid phase is denoted as the σ-phase).

Assuming incompressible flow, the total mass and momentum balance equations at the pore-scale are given by

$$\nabla \cdot \mathbf{v} = 0, \quad \text{in the } \beta\text{-phase}, \tag{1a}$$

$$\rho \frac{\partial \mathbf{v}}{\partial t} + \rho \mathbf{v} \cdot \nabla \mathbf{v} = -\nabla p + \rho \mathbf{g} + \nabla \cdot \left[\mu(\Gamma) \left(\nabla \mathbf{v} + \nabla \mathbf{v}^T \right) \right], \quad \text{in the } \beta\text{-phase}. \tag{1b}$$

In the above equations, $\mathbf{v}$ and p represent the fluid velocity and pressure, respectively, whereas ρ and $\mathbf{g}$ are the fluid density and the gravity acceleration vector. Finally, a generalized Newton's law of viscosity is used for the viscous stress tensor, so that the apparent viscosity, $\mu(\Gamma)$, depends on the strain-rate modulus (see, for example Chapter 2 in [54])

$$\Gamma = \sqrt{2\,(\mathbf{D} : \mathbf{D})}. \tag{2}$$

Here, $\mathbf{D}$ is the strain-rate (or rate of deformation) tensor, defined as

$$\mathbf{D} = \frac{1}{2} \left(\nabla \mathbf{v} + \nabla \mathbf{v}^T \right). \tag{3}$$

This formalism allows studying a variety of non-Newtonian flows such as the power-law model or the Carreau model and, in order to keep generality in modeling, it is convenient to not substitute any particular model for μ at the moment. Moreover, generality is also kept by considering that slip effects may be significant at the solid–fluid interface. This condition is relevant when, for instance, a significant roughness is present at the solid boundary so that an effective slip boundary condition can be derived and applied at an equivalent smooth surface. This type of approach was employed for Newtonian flow in the creeping [55] and, more generally, in the laminar regime [56] leading, at the first order of the roughness to macroscopic characteristic length-scale ratio, to a generalized Navier-type (or Maxwell) slip boundary condition (see [57,58]). Carrying out a formal development of such an effective boundary condition in the case of a non-Newtonian flow is out of the scope of the present work. However, for non-Newtonian flow, a similar first-order slip condition shall be adopted as justified in [59,60], namely

$$\mathbf{v} = -S\mathbf{P} \cdot \left(\mathbf{n} \cdot \left(\nabla \mathbf{v} + \nabla \mathbf{v}^T \right) \right), \quad \text{at } \mathscr{A}_{\beta\sigma}. \tag{4}$$

Here, $\mathbf{n}$ is the unit normal vector directed from the fluid phase towards the solid phase and $\mathbf{P}$ denotes the projection tensor onto the tangential plane at the solid–fluid interface $\mathscr{A}_{\beta\sigma}$, given by

$$\mathbf{P} = \mathbf{I} - \mathbf{nn}, \tag{5}$$

$\mathbf{I}$ being the identity tensor. As in the rest of the article, two juxtaposed vectors or tensors denote the outer product between these two quantities, which means, here, that $\mathbf{nn} \equiv \mathbf{n} \otimes \mathbf{n}$ is the dyadic formed with $\mathbf{n}$ and $\mathbf{n}$. In addition, S is the slip length, *i.e.*, the fictitious penetration distance in the solid phase beneath $\mathscr{A}_{\beta\sigma}$ where the no-slip condition would be applicable (see, for example [61]). As far as generalized Newtonian fluid flow is concerned, this parameter is expected to be a function, yet to be made explicit, of the local value of $\mathbf{D}$, and this is compliant with the fact that the viscosity solely depends on this parameter [59]. Moreover, S should also depend on the characteristic height of the asperities, δ_s, *i.e.*, $S = S(\mathbf{D}, \delta_s)$. The above formal slip velocity expression contains all the expected dependence on the physical features of the flow. As will be clear in the developments that follow, it is unnecessary to explicitly specify this dependence for the rest of the derivations. Finally, notice that equation Eq. (4) implies that no mass transport takes place between the solid and fluid phases since the normal projection of the velocity at the interface is zero.

The pore-scale problem statement is completed with boundary conditions at the macroscopic boundaries and by the initial condition. Since the analysis is focused on the porous medium bulk, the former are not necessary whereas the latter is assumed to be known and can be written as follows

$$\mathbf{v} = \mathbf{v}_0, \quad \text{when } t = 0. \tag{6}$$

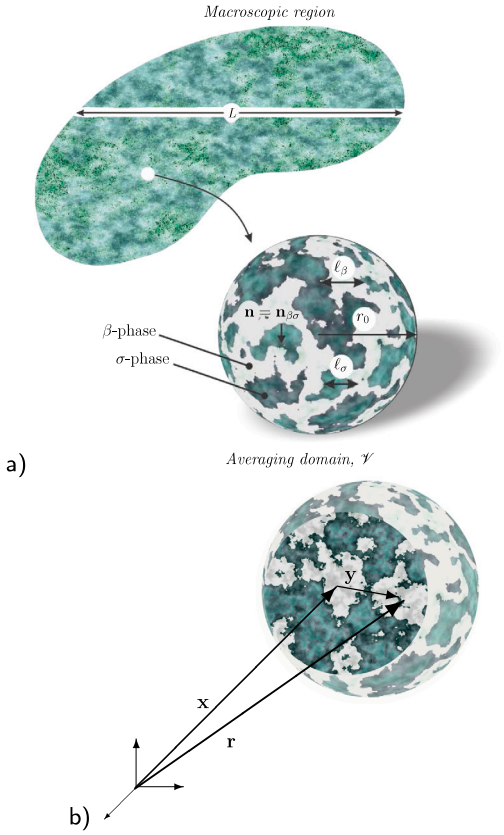

Fig. 1. a) Sketch of a porous medium saturated by a single fluid phase and of an averaging domain, including the main length scales. b) Position vectors locating the centroid of the averaging domain ($\mathbf{x}$) and points in the fluid phase relative to a fixed coordinate system ($\mathbf{r}$) and relative to $\mathbf{x}$ ($\mathbf{y}$).

3. Essential elements for upscaling

For the developments that follow, it is convenient to list the main elements useful for the derivation of the upscaled mass and momentum balance equations. To this end, consider an averaging domain $\mathscr{V}$ (of measure V), such as the one sketched in Fig. 1a), that contains portions of the solid and fluid phases. The averaging domain is assumed to be representative, in the sense that it contains all the essential structural information of the pore space that allows defining average quantities of interest to describe flow at the macroscopic scale. In particular, this implies that its characteristic size, r_0, is much larger than the maximum characteristic length associated to transport at the pore-scale (*i.e.*, $\ell_\mu = \max(\ell_\beta, \ell_\sigma)$; see Fig. 1a) and, at the same time, it is much smaller than the minimum length scale, L, associated to the macroscale. This is expressed as,

$$\ell_\mu \ll r_0 \ll L. \tag{7}$$

Macroscopic quantities over $\mathscr{V}$ can be expressed in terms of the *superficial averaging operator*. For a piece-wise continuous quantity, ψ, defined everywhere in the fluid phase, it is given by [48]

$$\langle \psi \rangle = \frac{1}{V} \int_{\mathscr{V}_\beta} \psi \, dV, \tag{8a}$$

$\mathscr{V}_\beta$, of measure V_β, being the domain occupied by the β-phase within $\mathscr{V}$. This averaging operator is the preferred one for the macroscale fluid velocity (also known as the Darcy or seepage velocity). However, for the pressure it is more convenient to use the *intrinsic averaging operator*, defined as follows

$$\langle \psi \rangle^\beta = \frac{1}{V_\beta} \int_{\mathscr{V}_\beta} \psi \, dV. \tag{8b}$$

The two averaging operators are related by

$$\langle\psi\rangle = \varepsilon\langle\psi\rangle^{\beta}, \tag{8c}$$

where $\varepsilon = V_\beta/V$ is the volume fraction of the fluid phase in the averaging domain, corresponding, in the present case, to the porosity. Moreover, since the porous medium geometry is assumed to be rigid and spatially homogeneous, it follows that ε can be treated as a constant in the developments that follow.

At this point, it is pertinent to direct the attention to the position vectors depicted in Fig. 1b), which are used to locate the centroid of the averaging domain, $\mathbf{x}$, and points in the fluid phase relative to a fixed system of coordinates, $\mathbf{r}$, and to $\mathbf{x}$, namely, $\mathbf{y}$. Since $\mathbf{r} = \mathbf{x} + \mathbf{y}$, it follows that the integrands in the averaging operators are evaluated at $\mathbf{r}$, while the integration step is performed over $\mathbf{y}$ so that the resulting average quantities are evaluated at $\mathbf{x}$. The explicit spatial dependence of pore-scale and average quantities is omitted in the rest of the text for the sake of simplicity in presentation.

Another element of the volume averaging method is the *spatial averaging theorem* (see, for instance, [62]), which allows interchanging spatial differentiation and integration. For the divergence operator of a continuous differentiable vectorial or tensorial function, ψ, it can be written as

$$\langle\nabla\cdot\psi\rangle = \nabla\cdot\langle\psi\rangle + \frac{1}{V}\int_{\mathscr{A}_{\beta\sigma}} \mathbf{n}\cdot\psi \; dA. \tag{9}$$

Furthermore, the spatial decomposition of pore-scale quantities into their corresponding intrinsic average and spatial deviations, as proposed in [63], is also of interest and is defined as follows

$$\psi = \langle\psi\rangle^{\beta} + \tilde{\psi}. \tag{10}$$

Since $\langle\psi\rangle^{\beta}$ is evaluated at $\mathbf{x}$ this allows treating average quantities as constants within $\mathscr{V}$ and leads, as a corollary, to the following average constraint for the spatial deviations

$$\langle\tilde{\psi}\rangle^{\beta} = 0. \tag{11}$$

As shown below, the derivation of the upscaled momentum transport equation deviates from the classical volume averaging method and borrows elements of the adjoint homogenization approach (see, *e.g.*, [47]). In particular, the following versions of Green's formulas are useful

$$\begin{aligned}
&\int_{\mathscr{V}_\beta} \left[\mathbf{a}\cdot\left(d\mathbf{c}\cdot\nabla\mathbf{B} - \nabla\mathbf{b} + \nabla\cdot\left[c\left(\nabla\mathbf{B} + \nabla\mathbf{B}^{T1}\right)\right]\right)\right.\\
&\qquad \left. -\left(-d\mathbf{c}\cdot\nabla\mathbf{a} - \nabla a + \nabla\cdot\left[c\left(\nabla\mathbf{a} + \nabla\mathbf{a}^{T}\right)\right]\right)\cdot\mathbf{B}\right]\; dV\\
&-\int_{\mathscr{V}_\beta} \left(\nabla\cdot\mathbf{ab} - d\nabla\cdot\mathbf{ca}\cdot\mathbf{B} - a\nabla\cdot\mathbf{B}\right)\; dV\\
&=\int_{\mathscr{A}_\beta} \left[\mathbf{a}\cdot\left(\mathbf{n}\cdot\left(-\mathbf{l}\mathbf{b} + c\left(\nabla\mathbf{B} + \nabla\mathbf{B}^{T1}\right)\right)\right)\right.\\
&\qquad \left. -\mathbf{n}\cdot\left(-d\mathbf{ca} - \mathbf{l}a + c\left(\nabla\mathbf{a} + \nabla\mathbf{a}^{T}\right)\right)\cdot\mathbf{B}\right]\; dA,
\end{aligned} \tag{12a}$$

$$\begin{aligned}
&\int_{\mathscr{V}_\beta} \left[\mathbf{A}^{T}\cdot\left(d\mathbf{c}\cdot\nabla\mathbf{B} - \nabla\mathbf{b} + \nabla\cdot\left[c\left(\nabla\mathbf{B} + \nabla\mathbf{B}^{T1}\right)\right]\right)\right.\\
&\qquad \left. -\left(-d\mathbf{c}\cdot\nabla\mathbf{A} - \nabla\mathbf{a} + \nabla\cdot\left[c\left(\nabla\mathbf{A} + \nabla\mathbf{A}^{T1}\right)\right]\right)^{T}\cdot\mathbf{B}\right]\; dV\\
&+\int_{\mathscr{V}_\beta} \left(d\nabla\cdot\mathbf{c}\mathbf{A}^{T}\cdot\mathbf{B} - \nabla\cdot\mathbf{Ab} + \mathbf{a}\nabla\cdot\mathbf{B}\right)\; dV\\
&=\int_{\mathscr{A}_\beta} \left[\mathbf{A}^{T}\cdot\left(\mathbf{n}\cdot\left(-\mathbf{l}\mathbf{b} + c\left(\nabla\mathbf{B} + \nabla\mathbf{B}^{T1}\right)\right)\right)\right.\\
&\left. -\left(\mathbf{n}\cdot\left(-d\mathbf{cA} - \mathbf{l}\mathbf{a} + c\left(\nabla\mathbf{A} + \nabla\mathbf{A}^{T1}\right)\right)\right)^{T}\cdot\mathbf{B}\right]\; dA,
\end{aligned} \tag{12b}$$

$$\begin{aligned}
&\int_{\mathscr{V}_\beta} \left[\mathbf{a}\cdot\left(d\mathbf{c}\cdot\nabla\mathbf{b} - \nabla b + \nabla\cdot c\left(\nabla\mathbf{b} + \nabla\mathbf{b}^{T}\right)\right)\right.\\
&\qquad \left. -\left(-d\mathbf{c}\cdot\nabla\mathbf{a} - \nabla a + \nabla\cdot c\left(\nabla\mathbf{a} + \nabla\mathbf{a}^{T}\right)\right)\cdot\mathbf{b}\right]\; dV\\
&-\int_{\mathscr{V}_\beta} \left(b\nabla\cdot\mathbf{a} - d\nabla\cdot\mathbf{ca}\cdot\mathbf{b} - a\nabla\cdot\mathbf{b}\right)\; dV\\
&=\int_{\mathscr{A}_\beta} \left[\mathbf{a}\cdot\left(\mathbf{n}\cdot\left(d\mathbf{cb} - \mathbf{l}b + c\left(\nabla\mathbf{b} + \nabla\mathbf{b}^{T}\right)\right)\right)\right.\\
&\qquad \left. -\left(\mathbf{n}\cdot\left(-\mathbf{l}a + c\left(\nabla\mathbf{a} + \nabla\mathbf{a}^{T}\right)\right)\right)\cdot\mathbf{b}\right]\; dA.
\end{aligned} \tag{12c}$$

In the above equations, $\mathscr{A}_\beta$ denotes the bounding surfaces enclosing $\mathscr{V}_\beta$. In addition, a, b and c are scalar fields, d is a constant scalar, whereas $\mathbf{a}$, $\mathbf{b}$ and $\mathbf{c}$ are vector fields and, finally, $\mathbf{A}$ and $\mathbf{B}$ are second-order tensor fields. All these quantities are arbitrary and are supposed to have the appropriate required regularities. In addition, the superscript $T1$ is used to indicate the permutation of the first two indices of a third-order tensor. Proofs of these formulas are provided in Appendix A.

4. Upscaling

In this section, the derivation of the macroscopic momentum balance equation is detailed by departing from the pore-scale formulation. For mass conservation, the classical volume averaging approach can be followed. The steps are identical to those reported in [51], leading to the following macroscopic mass balance equation

$$\nabla\cdot\langle\mathbf{v}\rangle = 0. \tag{13}$$

This is possible because, despite the presence of interfacial slip, it is nevertheless true that $\mathbf{n}\cdot\mathbf{v} = 0$ at $\mathscr{A}_{\beta\sigma}$ since the solid phase is assumed immobile and there is no mass transport between the fluid and solid phases (see [52,64]).

The macroscopic momentum balance is derived using a simplified version of the volume averaging method that makes use of some elements of the adjoint method reported above. This contrasts with the methodology used in [51] as it relies on Green's functions formalism. Since both, the pore-scale flow problem and the upscaling approach are different from previous works, it is pertinent to present the derivations in full detail. This is done in the following paragraphs.

To begin the derivations, it is convenient to consider that the porous medium can be represented by a spatially periodic structure. This assumption is classical in many upscaling techniques. Whereas it is usually a prerequisite adopted while formulating the pore-scale problem in the homogenization method [53], it is part of the development at the closure level while using volume averaging [48]. Nevertheless, a periodic unit cell representative of the process does not necessarily have to correspond to the smallest one required to reconstruct the geometrical structure (*i.e.*, the geometrical unit cell). Indeed, in order to not artificially constrain the physical behavior of the system with periodic conditions, a representative domain may require several geometrically periodic unit cells. This is the case, for instance, for (Newtonian) inertial flow at a Reynolds number larger than that characteristic of the first Hopf bifurcation [65]. Retaining this periodicity hypothesis, the flow problem in a periodic unit cell representative of the process can be written as follows

$$\nabla\cdot\mathbf{v} = 0, \quad \text{in } \mathscr{V}_\beta, \tag{14a}$$

$$\rho\frac{\partial\mathbf{v}}{\partial t} + \rho\mathbf{v}\cdot\nabla\mathbf{v} = -\nabla\tilde{p} - \nabla\langle p\rangle^{\beta} + \rho\mathbf{g} + \nabla\cdot\left[\mu(\Gamma)\left(\nabla\mathbf{v} + \nabla\mathbf{v}^{T}\right)\right], \quad \text{in } \mathscr{V}_\beta, \tag{14b}$$

$$\mathbf{v} = -S\mathbf{P}\cdot\left(\mathbf{n}\cdot\left(\nabla\mathbf{v} + \nabla\mathbf{v}^{T}\right)\right), \quad \text{at } \mathscr{A}_{\beta\sigma}, \tag{14c}$$

$$\psi(\mathbf{r} + \mathbf{l}_i) = \psi(\mathbf{r}), \quad i = 1,2,3; \; \psi = \mathbf{v}, \tilde{p}, \tag{14d}$$

$$\langle\tilde{p}\rangle^{\beta} = 0, \tag{14e}$$

$$\mathbf{v} = \mathbf{v}_0, \quad \text{when } t = 0. \tag{14f}$$

In the above equations, $\mathscr{V}_\beta$ and $\mathscr{A}_{\beta\sigma}$ now represent the domain occupied by the fluid phase and the solid–fluid interface in a periodic unit cell, respectively. Note that the spatial decomposition defined in Eq. (9) was used for the fluid pressure in Eq. (14b). This is done

because p cannot be assumed to be periodic in the unit cell. However, the pressure deviations, as well as the fluid velocity, can reasonably be considered as periodic fields, as indicated in Eq. (14d). Finally, the average constraint expressed in Eq. (11) and given in Eq. (14e) is necessary in order to have a well-posed problem. Certainly, the fact that Gray's decomposition is only used for the pressure and not for the velocity is a noticeable difference with respect to the classical volume averaging method as described in Chapter 4 in [48]. In the cited approach, the pore-scale momentum balance equation is averaged and, with the aid of the spatial averaging theorem and Gray's decomposition an unclosed model is derived, which is later redefined after a closure solution is found. In this work, a simplified version of the volume averaging method is used that only requires the flow problem solution in a periodic unit cell in terms of the physical sources. This solution can be subsequently averaged in order to obtain the corresponding macroscopic model as it is shown below.

Although the derivations can be performed in the time domain, it is convenient to continue working in the Laplace or in the Fourier domain. The use of the Laplace transform is a modeling choice that is made as it is slightly lighter in terms of notation and formalism in the direct and inverse transforms than the Fourier transform. However, either approach leads to the same equations after returning to the time domain. Certainly, the first obstacle in the application of the Laplace transform is the presence of nonlinear terms in the momentum transport equation, which is also an obstacle in the time domain analysis as discussed in [51]. Following the idea put forth in this work to overcome this issue, it is assumed that the velocity at any given time t appearing in the convective term, in the apparent viscosity coefficient and in the slip length, is available at a time $t - \Delta t$. Since Δt can be as small as required, it is reasonable to propose that $\mathbf{v}|_t \approx \mathbf{v}|_{t-\Delta t} \equiv \mathbf{v}_\Delta$ from a 0th order Taylor expansion. In this way, a linearization can be performed in an explicit manner by taking $\mathbf{v} = \mathbf{v}_\Delta$ for the convective velocity in the momentum equation and in the evaluation of Γ. Consequently, Eqs. (14b) and (14c) can be written as follows

$$\rho\frac{\partial \mathbf{v}}{\partial t} + \rho\mathbf{v}_\Delta\cdot\nabla\mathbf{v} = -\nabla p + \rho\mathbf{g} + \nabla\cdot\left[\mu(\Gamma_\Delta)\left(\nabla\mathbf{v} + \nabla\mathbf{v}^T\right)\right], \quad \text{in } \mathscr{V}_\beta, \tag{15a}$$

$$\mathbf{v} = -S_\Delta\mathbf{P}\cdot\left(\mathbf{n}\cdot\left(\nabla\mathbf{v} + \nabla\mathbf{v}^T\right)\right), \quad \text{at } \mathscr{A}_{\beta\sigma}. \tag{15b}$$

Here, $\Gamma_\Delta = \sqrt{2(\mathbf{D}_\Delta : \mathbf{D}_\Delta)}$, with $\mathbf{D}_\Delta = (\nabla\mathbf{v}_\Delta + \nabla\mathbf{v}_\Delta^T)/2$ and $S_\Delta = S(\mathbf{D}_\Delta, \delta_s)$. Note that quantities with the subscript Δ can be treated as known quantities independent of t. In this way, the flow problem in a unit cell can be written in the Laplace domain as follows

$$\nabla\cdot\hat{\mathbf{v}} = 0, \quad \text{in } \mathscr{V}_\beta, \tag{16a}$$

$$\rho s\hat{\mathbf{v}} + \rho\mathbf{v}_\Delta\cdot\nabla\hat{\mathbf{v}} = -\nabla\hat{\tilde{p}} - \underbrace{\left(\nabla\langle\hat{p}\rangle^\beta - \frac{\rho}{s}\mathbf{g} - \rho\mathbf{v}_0\right)}_{source} + \nabla\cdot\left[\mu(\Gamma_\Delta)\left(\nabla\hat{\mathbf{v}} + \nabla\hat{\mathbf{v}}^T\right)\right], \quad \text{in } \mathscr{V}_\beta, \tag{16b}$$

$$\hat{\mathbf{v}} = -S_\Delta\mathbf{P}\cdot\left(\mathbf{n}\cdot\left(\nabla\hat{\mathbf{v}} + \nabla\hat{\mathbf{v}}^T\right)\right), \quad \text{at } \mathscr{A}_{\beta\sigma}, \tag{16c}$$

$$\psi(\mathbf{r} + \mathbf{l}_i) = \psi(\mathbf{r}), \quad i = 1,2,3;\ \psi = \hat{\mathbf{v}}, \hat{\tilde{p}}, \tag{16d}$$

$$\left\langle\hat{\tilde{p}}\right\rangle^\beta = 0, \tag{16e}$$

in which $\hat{\mathbf{v}}$, $\hat{p}$ and $\hat{\tilde{p}}$ represent the Laplace transform of $\mathbf{v}$, p and $\tilde{p}$, respectively, while s is the frequency parameter.

At this point, one may follow the approach reported in [51] and propose a solution to the above problem. Nevertheless, due to the non linearity of the problem, it is beneficial to follow a more formal approach that relies upon Green's functions formalism. To this end, it is convenient to introduce the adjoint velocity pair of Green's functions in the Laplace domain, $\hat{\mathbf{G}}_a$ and $\hat{\mathbf{g}}_a$, which solve the following boundary-problem

$$\nabla\cdot\hat{\mathbf{G}}_a = \mathbf{0}, \quad \text{in } \mathscr{V}_\beta, \tag{17a}$$

$$\rho s\hat{\mathbf{G}}_a - \rho\mathbf{v}_\Delta\cdot\nabla\hat{\mathbf{G}}_a = -\nabla\hat{\mathbf{g}}_a + \nabla\cdot\left[\mu(\Gamma_\Delta)\left(\nabla\hat{\mathbf{G}}_a + \nabla\hat{\mathbf{G}}_a^{T1}\right)\right] + \delta(\mathbf{r} - \mathbf{r}_0)\mathbf{I}, \quad \text{in } \mathscr{V}_\beta, \tag{17b}$$

$$\hat{\mathbf{G}}_a = -S_\Delta\mathbf{P}\cdot\left(\mathbf{n}\cdot\left(\nabla\hat{\mathbf{G}}_a + \nabla\hat{\mathbf{G}}_a^{T1}\right)\right), \quad \text{at } \mathscr{A}_{\beta\sigma}, \tag{17c}$$

$$\psi(\mathbf{r} + \mathbf{l}_i) = \psi(\mathbf{r}), \quad i = 1,2,3;\ \psi = \hat{\mathbf{G}}_a, \hat{\mathbf{g}}_a, \tag{17d}$$

$$\hat{\mathbf{g}}_a = \mathbf{0}, \quad \text{at } \mathbf{r} = \mathbf{r}_a. \tag{17e}$$

In Eq. (17b), $\delta(\mathbf{r} - \mathbf{r}_0)$ is the Dirac delta function concentrated at $\mathbf{r}_0$, which is a position vector within the same domain as $\mathbf{r}$. In addition, in Eq. (17e), $\mathbf{r}_a$ is an arbitrary position vector located in the fluid phase.

It is now possible to find the relationship between $\hat{\mathbf{v}}$ and the source terms. This can be accomplished by using Green's formula in the form given in Eq. (12a). Setting $\mathbf{a} = \hat{\mathbf{v}}$, $\mathbf{c} = \mathbf{v}_\Delta$, $a = \hat{\tilde{p}}$, $\mathbf{b} = \hat{\mathbf{g}}_a$, $\mathbf{B} = \hat{\mathbf{G}}_a$, $c = \mu(\Gamma_\Delta)$ and $d = \rho$ and taking into account the solenoidal nature of $\hat{\mathbf{v}}$, $\mathbf{v}_\Delta$ and $\hat{\mathbf{G}}_a$, leads to

$$\begin{aligned}
&\int_{\mathscr{V}_\beta}\Big[\hat{\mathbf{v}}\cdot\Big(\rho\mathbf{v}_\Delta\cdot\nabla\hat{\mathbf{G}}_a - \nabla\hat{\mathbf{g}}_a + \nabla\cdot\Big[\mu(\Gamma_\Delta)\Big(\nabla\hat{\mathbf{G}}_a + \nabla\hat{\mathbf{G}}_a^{T1}\Big)\Big]\Big)\\
&-\Big(-\rho\mathbf{v}_\Delta\cdot\nabla\hat{\mathbf{v}} - \nabla\hat{\tilde{p}} + \nabla\cdot\left[\mu(\Gamma_\Delta)\left(\nabla\hat{\mathbf{v}} + \nabla\hat{\mathbf{v}}^T\right)\right]\Big)\cdot\hat{\mathbf{G}}_a\Big]\,dV\\
&= \int_{\mathscr{A}_\beta}\Big[\hat{\mathbf{v}}\cdot\Big(\mathbf{n}\cdot\Big(-\mathbf{I}\hat{\mathbf{g}}_a + \mu(\Gamma_\Delta)\Big(\nabla\hat{\mathbf{G}}_a + \nabla\hat{\mathbf{G}}_a^{T1}\Big)\Big)\Big)\\
&-\mathbf{n}\cdot\left(-\rho\mathbf{v}_\Delta\hat{\mathbf{v}} - \mathbf{I}\hat{\tilde{p}} + \mu(\Gamma_\Delta)\left(\nabla\hat{\mathbf{v}} + \nabla\hat{\mathbf{v}}^T\right)\right)\cdot\hat{\mathbf{G}}_a\Big]\,dA.
\end{aligned} \tag{18}$$

After substitution of equivalent expressions extracted from the momentum Eqs. (16b) and (17b) in the volume integral, this gives

$$\begin{aligned}
&\int_{\mathscr{V}_\beta}\Big[\hat{\mathbf{v}}\cdot\Big(\rho s\hat{\mathbf{G}}_a - \delta(\mathbf{r} - \mathbf{r}_0)\mathbf{I}\Big)\\
&\quad-\Big(\rho s\hat{\mathbf{v}} + \nabla\langle\hat{p}\rangle^\beta - \frac{\rho}{s}\mathbf{g} - \rho\mathbf{v}_0\Big)\cdot\hat{\mathbf{G}}_a\Big]\,dV =\\
&-\int_{\mathscr{A}_{\beta\sigma}}\mathbf{n}\cdot\hat{\mathbf{v}}\hat{\mathbf{g}}_a\,dA + \int_{\mathscr{A}_{\beta\sigma}}\mathbf{n}\cdot\left(\rho\mathbf{v}_\Delta\hat{\mathbf{v}} + \hat{\tilde{p}}\mathbf{I}\right)\cdot\hat{\mathbf{G}}_a\,dA\\
&+\int_{\mathscr{A}_{\beta\sigma}}\mu(\Gamma_\Delta)\,\mathbf{n}\cdot\Big(\hat{\mathbf{v}}\cdot\Big(\nabla\hat{\mathbf{G}}_a + \nabla\hat{\mathbf{G}}_a^{T1}\Big)\\
&\qquad-\left(\nabla\hat{\mathbf{v}} + \nabla\hat{\mathbf{v}}^T\right)\cdot\hat{\mathbf{G}}_a\Big)\,dA.
\end{aligned} \tag{19}$$

Note that, due to periodicity, the area integral reduces to the one over $\mathscr{A}_{\beta\sigma}$. Taking into account the boundary conditions in Eqs. (16c) and (17c), the two first integrals on the right hand side of the above relationship are zero due to the tangential character of $\hat{\mathbf{v}}$, $\mathbf{v}_\Delta$ and $\hat{\mathbf{G}}_a$ at $\mathscr{A}_{\beta\sigma}$. Moreover, the last area integral is also zero; the proof is provided in Appendix A in [52]. After little rearrangement, the above equation hence leads to the following result

$$\hat{\mathbf{v}} = -\int_{\mathscr{V}_\beta}\hat{\mathbf{G}}_a^T\,dV\cdot\left(\nabla\langle\hat{p}\rangle^\beta - \frac{\rho}{s}\mathbf{g}\right) + \rho\int_{\mathscr{V}_\beta}\hat{\mathbf{G}}_a^T\cdot\mathbf{v}_0\,dV. \tag{20}$$

At this point, it is convenient to introduce another Green's functions pair $\hat{\mathbf{G}}_v$ and $\hat{\mathbf{g}}_v$, which solves the following boundary-value problem in the Laplace domain

$$\nabla\cdot\hat{\mathbf{G}}_v = \mathbf{0}, \quad \text{in } \mathscr{V}_\beta, \tag{21a}$$

$$\rho s\hat{\mathbf{G}}_v + \rho\mathbf{v}_\Delta\cdot\nabla\hat{\mathbf{G}}_v = -\nabla\hat{\mathbf{g}}_v + \nabla\cdot\left[\mu(\Gamma_\Delta)\left(\nabla\hat{\mathbf{G}}_v + \nabla\hat{\mathbf{G}}_v^{T1}\right)\right] + \delta(\mathbf{r} - \mathbf{r}_0)\mathbf{I}, \quad \text{in } \mathscr{V}_\beta, \tag{21b}$$

$$\hat{\mathbf{G}}_v = -S_\Delta\mathbf{P}\cdot\left(\mathbf{n}\cdot\left(\nabla\hat{\mathbf{G}}_v + \nabla\hat{\mathbf{G}}_v^{T1}\right)\right), \quad \text{at } \mathscr{A}_{\beta\sigma}, \tag{21c}$$

$$\psi(\mathbf{r} + \mathbf{l}_i) = \psi(\mathbf{r}), \quad i = 1,2,3;\ \psi = \hat{\mathbf{G}}_v, \hat{\mathbf{g}}_v, \tag{21d}$$

$$\hat{\mathbf{g}}_v = \mathbf{0}, \quad \text{at } \mathbf{r} = \mathbf{r}_a. \tag{21e}$$

Note that the above problem on $\hat{\mathbf{G}}_v$ and $\hat{\mathbf{g}}_v$ only differs from the adjoint problem given in Eqs. (17) by the sign on the convective-like acceleration term in the momentum equation. This sign change is convenient, because standard Navier Stokes solvers can be used for its solution. Basically, g_{vi} and G_{vij} can be respectively interpreted as the pressure deviations and the velocity in the j-direction at a field point

located at $\mathbf{r}$, resulting from a singular force (a Stokeslet) placed at a source point $\mathbf{r}_0$ in the i-direction.

It is now of interest to determine the relationship between the adjoint and the new Green's functions pairs for the velocity. With this objective in mind, Green's formula in the form given in Eq. (12b) is applied, setting $\mathbf{a} = \hat{\mathbf{g}}_v$, $\mathbf{c} = \mathbf{v}_\Delta$, $\mathbf{A} = \hat{\mathbf{G}}_v$, $\mathbf{b} = \hat{\mathbf{g}}_a$, $\mathbf{B} = \hat{\mathbf{G}}_a$, $c = \mu(\Gamma_\Delta)$ and $d = \rho$. Taking into account the solenoidal nature of $\mathbf{v}_\Delta$, $\hat{\mathbf{G}}_v$ and $\hat{\mathbf{G}}_a$, this yields

$$\begin{aligned}
&\int_{\mathscr{V}_\beta}\Big[\hat{\mathbf{G}}_v^T\cdot\Big(\rho\mathbf{v}_\Delta\cdot\nabla\hat{\mathbf{G}}_a-\nabla\hat{\mathbf{g}}_a\\
&+\nabla\cdot\Big[\mu(\Gamma_\Delta)\Big(\nabla\hat{\mathbf{G}}_a+\nabla\hat{\mathbf{G}}_a^{T1}\Big)\Big]\Big)-\Big(-\rho\mathbf{v}_\Delta\cdot\nabla\hat{\mathbf{G}}_v-\nabla\hat{\mathbf{g}}_v\\
&+\nabla\cdot\Big[\mu(\Gamma_\Delta)\Big(\nabla\hat{\mathbf{G}}_v+\nabla\hat{\mathbf{G}}_v^{T1}\Big)\Big]\Big)^T\cdot\hat{\mathbf{G}}_a\Big]\,dV\\
&=\int_{\mathscr{A}_{\beta\sigma}}\Big[\hat{\mathbf{G}}_v^T\cdot\Big(\mathbf{n}\cdot\Big(-\mathbf{I}\hat{\mathbf{g}}_a+\mu(\Gamma_\Delta)\Big(\nabla\hat{\mathbf{G}}_a+\nabla\hat{\mathbf{G}}_a^{T1}\Big)\Big)\Big)\\
&\quad-\Big(\mathbf{n}\cdot\Big(-\rho\mathbf{v}_\Delta\hat{\mathbf{G}}_v-\mathbf{I}\hat{\mathbf{g}}_v\\
&\quad+\mu(\Gamma_\Delta)\Big(\nabla\hat{\mathbf{G}}_v+\nabla\hat{\mathbf{G}}_v^{T1}\Big)\Big)\Big)^T\cdot\hat{\mathbf{G}}_a\Big]\,dA,
\end{aligned}\tag{22}$$

in which the periodicity condition was considered, reducing the area integral to $\mathscr{A}_{\beta\sigma}$. Substituting the corresponding expressions from the momentum-like Eqs. (17b) and (21b) in the volume integral, the above equation leads to the following relationship

$$\begin{aligned}
-\hat{\mathbf{G}}_v^T+\hat{\mathbf{G}}_a=\int_{\mathscr{A}_{\beta\sigma}}\Big(-\Big(\hat{\mathbf{g}}_a\mathbf{n}\cdot\hat{\mathbf{G}}_v\Big)^T\\
+\rho\mathbf{n}\cdot\mathbf{v}_\Delta\hat{\mathbf{G}}_v^T\cdot\hat{\mathbf{G}}_a-\hat{\mathbf{g}}_v\mathbf{n}\cdot\hat{\mathbf{G}}_a\Big)\,dA.
\end{aligned}\tag{23}$$

To arrive at this result, expressions of $\hat{\mathbf{G}}_a$ and $\hat{\mathbf{G}}_v$ at the interface, given by Eqs. (17c) and (21c), were introduced in the area integral involving $\Big(\nabla\hat{\mathbf{G}}_a+\nabla\hat{\mathbf{G}}_a^{T1}\Big)$ and $\Big(\nabla\hat{\mathbf{G}}_v+\nabla\hat{\mathbf{G}}_v^{T1}\Big)$, showing that this part of the integral is zero. Taking into account the tangential character of $\hat{\mathbf{G}}_v$, $\mathbf{v}_\Delta$ and $\hat{\mathbf{G}}_v$ at $\mathscr{A}_{\beta\sigma}$, it clearly appears that all the terms on the right-hand side of Eq. (23) are also zero, finally yielding

$$\hat{\mathbf{G}}_a^T=\hat{\mathbf{G}}_v.\tag{24}$$

Consequently, the formal solution for $\hat{\mathbf{v}}$ given in Eq. (20) can now be expressed as

$$\hat{\mathbf{v}}=-\int_{\mathscr{V}_\beta}\hat{\mathbf{G}}_v\,dV\cdot\Big(\nabla\langle\hat{p}\rangle^\beta-\frac{\rho}{s}\mathbf{g}\Big)+\rho\int_{\mathscr{V}_\beta}\hat{\mathbf{G}}_v\cdot\mathbf{v}_0\,dV.\tag{25a}$$

For completeness, it is of interest to provide the formal solution for $\hat{p}$. Using a procedure similar to the one employed for $\hat{\mathbf{v}}$, the following result is obtained for the fluid pressure deviations in the Laplace domain (see details in Appendix B)

$$\hat{p}=-\int_{\mathscr{V}_\beta}\hat{\mathbf{g}}_v\,dV\cdot\Big(\nabla\langle\hat{p}\rangle^\beta-\frac{\rho}{s}\mathbf{g}\Big)+\rho\int_{\mathscr{V}_\beta}\hat{\mathbf{g}}_v\cdot\mathbf{v}_0\,dV+\varphi.\tag{25b}$$

Clearly, only the Green's function problem given for $\hat{\mathbf{G}}_v$ and $\hat{\mathbf{g}}_v$ (or $\mathbf{G}_v$ and $\mathbf{g}_v$ in the time domain) is required to be solved in order to obtain $\hat{\mathbf{v}}$ and $\hat{p}$ (or $\mathbf{v}$ and $\tilde{p}$). However, it is worth noting that the solution of this problem would imply the numerical solution of a Stokes-like problem with an infinite concentrated source located at $\mathbf{r}_0\in\mathscr{V}_\beta$. To avoid having to deal with this difficulty, it is convenient to define the following pair of closure variables

$$\frac{s\hat{\mathbf{F}}}{\mu_{ref}}=\int_{\mathscr{V}_\beta}\hat{\mathbf{G}}_v\,dV,\tag{26a}$$

$$s\hat{\mathbf{f}}=\int_{\mathscr{V}_\beta}\hat{\mathbf{g}}_v\,dV,\tag{26b}$$

with μ_{ref} being a reference viscosity. In the above equations, $\hat{\mathbf{f}}$ and $\hat{\mathbf{F}}$ were conveniently defined in order for the macroscopic velocity to take the form of Darcy's law, under steady-state conditions as shown in the following section. Note that the closure variables $\hat{\mathbf{F}}$ and $\hat{\mathbf{f}}$ are only functions of $\mathbf{r}$ since the $\mathbf{r}_0$ dependence is filtered out by the integration step. In this way, applying the volumetric integration operator with respect to $\mathbf{r}_0$ to Eqs. (21), taking into account the definitions given in Eqs. (26), leads to the following closure problem in the Laplace domain

$$\nabla\cdot\hat{\mathbf{F}}=\mathbf{0},\quad\text{in }\mathscr{V}_\beta,\tag{27a}$$

$$\begin{aligned}
&\frac{\rho}{\mu_{ref}}s\hat{\mathbf{F}}+\frac{\rho}{\mu_{ref}}\mathbf{v}_\Delta\cdot\nabla\hat{\mathbf{F}}=-\nabla\hat{\mathbf{f}}\\
&\qquad+\nabla\cdot\Big[\frac{\mu(\Gamma_\Delta)}{\mu_{ref}}\Big(\nabla\hat{\mathbf{F}}+\nabla\hat{\mathbf{F}}^{T1}\Big)\Big]+\frac{\mathbf{I}}{s},\quad\text{in }\mathscr{V}_\beta,
\end{aligned}\tag{27b}$$

$$\hat{\mathbf{F}}=-S_\Delta\mathbf{P}\cdot\Big(\mathbf{n}\cdot\Big(\nabla\hat{\mathbf{F}}+\nabla\hat{\mathbf{F}}^{T1}\Big)\Big),\quad\text{at }\mathscr{A}_{\beta\sigma},\tag{27c}$$

$$\psi(\mathbf{r}+\mathbf{l}_i)=\psi(\mathbf{r}),\quad i=1,2,3;\ \psi=\hat{\mathbf{F}},\hat{\mathbf{f}},\tag{27d}$$

$$\hat{\mathbf{f}}=\mathbf{0},\quad\text{at }\mathbf{r}=\mathbf{r}_a.\tag{27e}$$

It should be pointed out that to arrive at the formulation of the above problem, integration and spatial derivation were permuted since the latter is with respect to $\mathbf{r}$.

The macroscopic momentum balance equation results from applying the superficial averaging operator on both sides of Eq. (25a) and this yields

$$\langle\hat{\mathbf{v}}\rangle=-\frac{s\hat{\mathbf{H}}_\mu}{\mu_{ref}}\cdot\Big(\nabla\langle\hat{p}\rangle^\beta-\frac{\rho}{s}\mathbf{g}\Big)+\frac{\rho}{\mu_{ref}}\Big\langle s\hat{\mathbf{F}}\cdot\mathbf{v}_0\Big\rangle.\tag{28}$$

Here, the apparent permeability tensor in the Laplace domain is defined as

$$\hat{\mathbf{H}}_\mu=\Big\langle\hat{\mathbf{F}}\Big\rangle.\tag{29}$$

As a final step in the derivations, the inverse Laplace transform is applied on both sides of Eq. (28) to obtain the macroscopic momentum equation in the time domain that is given by

$$\begin{aligned}
\langle\mathbf{v}\rangle=&-\frac{1}{\mu_{ref}}\int_{t_0=0}^{t_0=t}\frac{d\mathbf{H}_\mu}{dt}\Big|_{t-t_0}\cdot\Big(\nabla\langle p\rangle^\beta-\rho\mathbf{g}\Big)\Big|_{t_0}\,dt_0\\
&+\frac{\rho}{\mu_{ref}}\Big\langle\frac{\partial\mathbf{F}}{\partial t}\cdot\mathbf{v}_0\Big\rangle.
\end{aligned}\tag{30}$$

Certainly, the above equation could have been reported in terms of an effective coefficient that represents $d\mathbf{H}_\mu/dt$ (see, for example, equation (4.42) in [47]). However, it is convenient to present it in its current form so that $\mathbf{H}_\mu$ has the units of permeability and can lead to Darcy's law under steady and non-inertial Newtonian flow conditions. The above is possible because of the definitions adopted in Eqs. (26). In addition, the corresponding closure problem in the time domain results from applying the inverse Laplace transform to Eqs. (27). This leads to

$$\nabla\cdot\mathbf{F}=\mathbf{0},\quad\text{in }\mathscr{V}_\beta,\tag{31a}$$

$$\begin{aligned}
&\frac{\rho}{\mu_{ref}}\frac{\partial\mathbf{F}}{\partial t}+\frac{\rho}{\mu_{ref}}\mathbf{v}\cdot\nabla\mathbf{F}=-\nabla\mathbf{f}\\
&\qquad+\nabla\cdot\Big[\frac{\mu(\Gamma)}{\mu_{ref}}\Big(\nabla\mathbf{F}+\nabla\mathbf{F}^{T1}\Big)\Big]+\mathbf{I},\quad\text{in }\mathscr{V}_\beta,
\end{aligned}\tag{31b}$$

$$\mathbf{F}=-S\mathbf{P}\cdot\Big(\mathbf{n}\cdot\Big(\nabla\mathbf{F}+\nabla\mathbf{F}^{T1}\Big)\Big),\quad\text{at }\mathscr{A}_{\beta\sigma},\tag{31c}$$

$$\psi(\mathbf{r}+\mathbf{l}_i)=\psi(\mathbf{r}),\quad i=1,2,3;\ \psi=\mathbf{F},\mathbf{f},\tag{31d}$$

$$\mathbf{f}=\mathbf{0},\quad\text{at }\mathbf{r}=\mathbf{r}_a,\tag{31e}$$

$$\mathbf{F}=\mathbf{0},\quad\text{when }t=0.\tag{31f}$$

Here, it must be emphasized that in Eqs. (31b) and (31c), the limit $\Delta t\to 0$ was taken so that $\mathbf{v}_\Delta\to\mathbf{v}$, $\mu(\Gamma_\Delta)\to\mu(\Gamma)$ and $S_\Delta\to S$. In addition, the initial condition was chosen to be in the form given in Eq. (31f), which is consistent with previous works (cf. [51,53]). Performing the

projection of the above problem onto each of the base vectors of the system of coordinates indicates that the corresponding projections of $\mathbf{F}$ and $\mathbf{f}$ respectively represent the velocity and pressure deviations resulting from a unit macroscopic pressure gradient in this direction. This is an agreement with the interpretation of $(\mathbf{G}_v, \mathbf{g}_v)$ given above. It is pertinent to remark that, due to the closure variables definitions given in Eqs. (26), the source term in Eq. (27b) is $\mathbf{I}/s$, which, in turn, leads to the source term $\mathbf{I}$ in the time domain version (see Eq. (31b)). This observation is relevant because it allows for the closure problem defined in Eqs. (31) to reduce, under non-inertial and steady-state conditions, to the one reported in Section 3 in [38].

It should be noted that the above closure problem could be written in a fully closed and nonlinear form, *i.e.*, in a version in which the pore-scale velocity no longer appears and is not required to be known *a priori*. This could be performed by introducing the formal solution for $\mathbf{v}$ deriving from Eq. (25a). However, this would be at the cost of a tremendously complicated problem to solve, and, from a practical point of view, it is more convenient to first solve the flow problem in a unit cell and then use the solution for $\mathbf{v}$ to solve the closure problem given in Eqs. (31). At this point, it is worth emphasizing the advantage of introducing the Green's function problem for $\mathbf{G}_v$ and $\mathbf{g}_v$. Indeed, this leads to the above closure problem in which the convective acceleration term has a positive sign, hence allowing the use of standard Navier–Stokes solvers. In the adjoint homogenization method, only the adjoint velocity Green's function pair is considered (see section 4.2 in [47]). As a consequence, the apparent permeability tensor is defined in terms of the transpose of the closure variable in this reference. In addition, it is worth mentioning that in the current formulation it is necessary to solve only one closure problem in order to predict the two effective-medium quantities involved in the macroscopic momentum equation. This is an advantage with respect to previous works (see, for example, [51]), in which two closure problems were required.

Finally, note that the non-Newtonian fluid rheology information contained in the original flow model is captured in the closure variables through $\mathbf{v}$, $\mu(\dot{\Gamma})$ and S. This information is later passed through spatial integration filters to compute the effective-medium quantities in Eq. (30). This passing of rheology information is analogous to the approach reported in [38] under steady-state conditions.

5. Macroscale model summary

In the previous sections, a macroscopic model for unsteady generalized Newtonian fluid flow in a rigid and homogeneous porous medium was derived. The assumptions on which it relies can be listed as follows. No mass transport takes place at the solid–fluid interface, whereas slip may occur that can be represented by a first-order (Navier-type) boundary condition. The flow is assumed incompressible and laminar, while the solid is seen as immobile. A unit cell, representative of the structure can be identified as part of an infinite periodic equivalent structure, that is used to determine the effective coefficients. In addition, the necessary disparity of characteristic length scales is assumed to exist between the pore-scale and the macroscale. On the basis of the above assumptions, the closed form of the macroscale model is composed of the following mass conservation equation

$$\nabla \cdot \langle \mathbf{v} \rangle = 0, \tag{32a}$$

whereas, the momentum transport equation is non-local in time and can be written as

$$\langle \mathbf{v} \rangle = \frac{1}{\mu_{ref}} \left(-\frac{d\mathbf{H}_\mu}{dt} * \cdot \left(\nabla \langle p \rangle^\beta - \rho \mathbf{g} \right) + \rho \boldsymbol{\alpha}_0 \right). \tag{32b}$$

Here, $* \cdot$ stands for the combined convolution and inner product. In this expression, the apparent permeability tensor in the time domain is defined as

$$\mathbf{H}_\mu = \langle \mathbf{F} \rangle, \tag{32c}$$

and, for compactness, the memory vector, $\boldsymbol{\alpha}_0$, is defined as

$$\boldsymbol{\alpha}_0 = \left\langle \frac{\partial \mathbf{F}}{\partial t} \cdot \mathbf{v}_0 \right\rangle. \tag{32d}$$

The first term on the right-hand side of the upscaled momentum equation, involving the convolution product between the time derivative of the apparent permeability tensor and the macroscopic forcing, accounts for viscous resistance with a memory effect on the macroscopic pressure gradient. The second term accounts for the memory effect of the initial flow condition. It should be mentioned that, since the closure problem solution contains information of the initial velocity field, the apparent permeability tensor also depends on the initial condition. Note that the structure of the macroscopic momentum balance equation is in agreement with those reported for Newtonian unsteady flow in rigid and homogeneous porous media in the creeping regime with interfacial slip [52], and with inertial effects but without slip [51,53].

The algorithm to compute the effective quantities $\mathbf{H}_\mu$ and $\boldsymbol{\alpha}_0$ is the following: (i) solve the flow problem (Eqs. (14)) in the unit cell to obtain both the viscosity and velocity fields; (ii) use these fields to solve the closure problem (Eqs. (31)) yielding the field of $\mathbf{F}$; (iii) compute $\mathbf{H}_\mu$ and $\boldsymbol{\alpha}_0$ from Eqs. (32c) and (32d), respectively.

Finally, an analysis of symmetry and positiveness of $\mathbf{H}_\mu$ can be performed in a way similar to that followed in section 3.3 of the work by Lasseux et al. [51] and Appendix C of [52]. A summary is provided in Appendix C. The result is that this tensor is, in general, not symmetric (see also [66]) and can be decomposed into its irreducible parts. In this way, the skew-symmetric contribution is shown to only result from inertia (*i.e.*, convective acceleration), while temporal acceleration and viscous effects contribute to the symmetric part. Moreover, $\hat{\mathbf{H}}_\mu$ is positive semi-definite. In particular, the apparent permeability tensor in steady-state conditions is positive semi-definite. Furthermore, since the closure problem depends on the macroscropic pressure gradient, the apparent permeability tensor is a non-trivial function of this driving force and consequently, Eq. (32b) is nonlinear with respect to $\nabla \langle p \rangle^\beta$.

It is worth mentioning that, under steady and creeping flow conditions, the left-hand side of Eq. (31b) can be omitted. Nevertheless, the closure variables still depend on the velocity field through the viscosity coefficient. Moreover, using the final value theorem (see, for example, Appendix D in [52]), it can be demonstrated that the dynamic momentum balance Eq. (32b) reduces to

$$\lim_{t \to \infty} \langle \mathbf{v} \rangle = -\frac{1}{\mu_{ref}} \mathbf{H}_\mu \cdot \left(\nabla \langle p \rangle^\beta - \rho \mathbf{g} \right), \tag{33}$$

when the forcing is steady after a given time, and this corresponds to the seepage velocity in Eq. (17) of the work by Airiau and Bottaro [38] in which $\mathbf{K}^C$ identifies as $\mathbf{H}_\mu$. In addition, it should be noted that once inertia and slip effects are disregarded in Eqs. (31), the ensuing closure problem, whose solution yields $\mathbf{H}_\mu$, reduces to Eqs. (10) (and associate boundary conditions) of the latter reference. This is consistent with the fact that the scale ratio $\epsilon = \ell_\mu / L$, as defined in the homogenization approach, is supposed to be vanishingly small in the context of an infinitely periodic medium assumed in the present development. As a result, the model obtained here reduces to that reported in [38] for the corresponding flow conditions.

For practical purposes, it may be of interest to combine the macroscopic mass and momentum balance Eqs. (32a) and (32b) yielding the following equation for the macroscopic pressure

$$\frac{d\mathbf{H}_\mu}{dt} *: \nabla \nabla \langle p \rangle^\beta = 0. \tag{34}$$

Here, $*:$ denotes the combined temporal convolution and double dot product. Note that in the above expression, the initial condition memory effect is filtered out. Nevertheless, the effect of $\mathbf{v}_0$ is still contained in $\mathbf{H}_\mu$. This equation may be used to determine the macroscopic pressure field $\langle p \rangle^\beta$ when appropriate macroscopic boundary conditions are specified. Subsequently, the macroscopic velocity field may be computed using Eq. (32b).

6. Results

The purpose of this section is twofold. First, the dynamics of the components of the apparent permeability tensor, $\mathbf{H}_\mu$, and of the memory vector, $\boldsymbol{\alpha}_0$, are analyzed under creeping and laminar flow conditions at a moderate Reynolds number value that remains smaller than the critical value corresponding to the first Hopf bifurcation [65]. Slip effects are not considered here (*i.e.*, in the following S is taken to be 0) to reduce the number of degrees of freedom. Such an analysis has been investigated in [52] in the Newtonian case. It is worth pointing out that the accuracy of the macroscale model derived here is not conditioned by the interfacial slip effects. This is due to the fact that no assumptions about them were invoked in the model derivation. Hence, for the sake of brevity in presentation, the analysis of slip effects is relegated to a separate study. Second, the macroscopic model predictions of the dynamics of the seepage velocity are validated by comparison with pore-scale simulations.

6.1. Dimensionless formulation

To commence the analysis, it is convenient to reformulate the microscale and macroscale models, as well as the closure problem, in a dimensionless form. To this end, the following definitions are adopted (the superscript * denotes dimensionless quantities)

$$\mathbf{v}^* = \frac{\mathbf{v}}{v_{ref}},\ \mathbf{v}_0^* = \frac{\mathbf{v}_0}{v_{ref}},\ p^* = \frac{p\ell}{v_{ref}\,\mu_{ref}},\ \mathbf{r}^* = \frac{\mathbf{r}}{\ell},$$
$$t^* = \frac{t}{t_{ref}},\ \mathbf{F}^* = \frac{\mathbf{F}}{\ell^2},\ \mathbf{f}^* = \frac{\mathbf{f}}{\ell},$$
$$\Gamma^* = \frac{\mu_{ref}}{\ell\|\nabla\mathscr{P}\|_{t=0}}\Gamma, \tag{35}$$

where ℓ represents the unit cell side length (see Fig. 2). In addition, the reference time is chosen to be $t_{ref} = \rho\ell^2/\mu_{ref}$ and the reference velocity is defined as

$$v_{ref} = \frac{\ell^2\|\nabla\mathscr{P}\|_{t=0}}{\mu_{ref}}. \tag{36}$$

Here, $\nabla\mathscr{P}|_t = \nabla\langle p\rangle^\beta\big|_t - \rho\mathbf{g}$ is the modified macroscopic pressure gradient, which, at $t = 0$, is the forcing of the initial flow that obeys the following dimensionless boundary-value problem in a periodic unit cell

$$\nabla^*\cdot\mathbf{v}_0^* = 0, \quad \text{in } \mathscr{V}_\beta, \tag{37a}$$
$$Re\mathbf{v}_0^*\cdot\nabla^*\mathbf{v}_0^* = -\nabla^*\tilde{p}_0^* - \nabla^*\mathscr{P}_0^* + \nabla^*\cdot\left[\frac{\mu(\Gamma_0^*)}{\mu_{ref}}\left(\nabla^*\mathbf{v}_0^* + \nabla^*\mathbf{v}_0^{*T}\right)\right], \quad \text{in } \mathscr{V}_\beta, \tag{37b}$$
$$\mathbf{v}_0^* = \mathbf{0}, \quad \text{at } \mathscr{A}_{\beta\sigma}, \tag{37c}$$
$$\psi(\mathbf{r}^* + \mathbf{l}_i^*) = \psi(\mathbf{r}^*), \quad i = 1,2,3;\ \psi = \mathbf{v}_0^*, \tilde{p}_0^*, \tag{37d}$$
$$\left\langle\tilde{p}_0^*\right\rangle^\beta = 0. \tag{37e}$$

In the above equations, the subscript 0 was included to make it explicit that the dependent variables are evaluated at $t = 0$. In addition, adopting a two-dimensional unit cell, the initial dimensionless macroscopic pressure gradient is given by

$$\nabla^*\mathscr{P}_0^* = -\cos\theta\mathbf{e}_x - \sin\theta\mathbf{e}_y. \tag{38}$$

In Eq. (37b), the cell Reynolds number, resulting from the scaling choices is given by

$$Re = \frac{\rho v_{ref}\,\ell}{\mu_{ref}}. \tag{39}$$

Note that this definition is not compliant with the typical one found in engineering applications that usually relies upon an effective viscosity, and requires assuming the classical 1D form of Darcy's law. As pointed out in [38], such an approach is not compatible with the formal upscaling method used in this work, which does not calls upon data fitting to predict the effective medium coefficients.

Furthermore, the dimensionless flow model in a periodic unit cell, according to Eqs. (14), is given by

$$\nabla^*\cdot\mathbf{v}^* = 0, \quad \text{in } \mathscr{V}_\beta, \tag{40a}$$
$$\frac{\partial\mathbf{v}^*}{\partial t^*} + Re\mathbf{v}^*\cdot\nabla^*\mathbf{v}^* = -\nabla^*\tilde{p}^* - \nabla^*\mathscr{P}^* + \nabla^*\cdot\left[\frac{\mu(\Gamma^*)}{\mu_{ref}}\left(\nabla^*\mathbf{v}^* + \nabla^*\mathbf{v}^{*T}\right)\right], \quad \text{in } \mathscr{V}_\beta, \tag{40b}$$
$$\mathbf{v}^* = \mathbf{0}, \quad \text{at } \mathscr{A}_{\beta\sigma}, \tag{40c}$$
$$\psi(\mathbf{r}^* + \mathbf{l}_i^*) = \psi(\mathbf{r}), \quad i = 1,2,3;\ \psi = \mathbf{v}^*, \tilde{p}^*, \tag{40d}$$
$$\langle\tilde{p}^*\rangle^\beta = 0, \tag{40e}$$
$$\mathbf{v}^* = \mathbf{v}_0^*, \quad \text{when } t^* = 0. \tag{40f}$$

In the developments that follow, $\nabla^*\mathscr{P}^*$ in Eq. (40b) is regarded as a known function of time, that is specified later on. Clearly, this problem *a priori* requires the solution of Eqs. (37) in order to account for the initial velocity. Once the above problem is solved, the velocity field is substituted into the dimensionless form of the closure problem given in Eqs. (31), which can be written as

$$\nabla^*\cdot\mathbf{F}^* = \mathbf{0}, \quad \text{in } \mathscr{V}_\beta, \tag{41a}$$
$$\frac{\partial\mathbf{F}^*}{\partial t^*} + Re\mathbf{v}^*\cdot\nabla^*\mathbf{F}^* = -\nabla^*\mathbf{f}^* + \nabla^*\cdot\left[\frac{\mu(\Gamma^*)}{\mu_{ref}}\left(\nabla^*\mathbf{F}^* + \nabla^*\mathbf{F}^{*T1}\right)\right] + \mathbf{I}, \quad \text{in } \mathscr{V}_\beta, \tag{41b}$$
$$\mathbf{F}^* = \mathbf{0}, \quad \text{at } \mathscr{A}_{\beta\sigma}, \tag{41c}$$
$$\psi(\mathbf{r}^* + \mathbf{l}_i^*) = \psi(\mathbf{r}^*), \quad i = 1,2,3;\ \psi = \mathbf{F}^*, \mathbf{f}^*, \tag{41d}$$
$$\mathbf{f}^* = \mathbf{0}, \quad \text{at } \mathbf{r}^* = \mathbf{r}_a^*, \tag{41e}$$
$$\mathbf{F}^* = \mathbf{0}, \quad \text{when } t^* = 0. \tag{41f}$$

Once this problem is solved, the field of $\mathbf{F}^*$ is used to compute the following dimensionless macroscopic quantities

$$\mathbf{H}_\mu^* \equiv \frac{\mathbf{H}_\mu}{\ell^2} = \langle\mathbf{F}^*\rangle, \tag{42a}$$
$$\boldsymbol{\alpha}_0^* \equiv \frac{\rho\boldsymbol{\alpha}_0}{\mu_{ref}v_{ref}} = \left\langle\frac{\partial\mathbf{F}^*}{\partial t^*}\cdot\mathbf{v}_0^*\right\rangle. \tag{42b}$$

They are subsequently substituted into the following dimensionless version of the macroscopic momentum balance equation

$$\langle\mathbf{v}^*\rangle = -\frac{d\mathbf{H}_\mu^*}{dt^*} * \cdot\nabla^*\mathscr{P}^* + \boldsymbol{\alpha}_0^*, \tag{43}$$

to compute the values of the macroscale velocity. At this point, it is worth recalling that, due to the non-linearities induced by the non-Newtonian nature of the fluid flow and by the inertial effects, $\mathbf{H}_\mu^*$ and $\boldsymbol{\alpha}_0^*$, depend on the macroscopic pressure gradients $\nabla^*\mathscr{P}_0^*$ and $\nabla^*\mathscr{P}^*$.

In the following paragraphs the analysis is focused on Carreau fluids, which obey the following constitutive equation

$$\mu(\Gamma) = \mu_\infty + (\mu_0 - \mu_\infty)\left[1 + (\lambda\Gamma)^2\right]^{(n-1)/2}. \tag{44a}$$

Here, μ_0, μ_∞, λ and n represent the zero- and infinite shear-rate viscosity coefficients, the relaxation time and the power-law index, respectively. As suggested in previously reported works [38,67,68], it is assumed that $\mu_{ref} = \mu_0$ and $\mu_\infty = 0$. Consequently,

$$\mu^*(\Gamma^*) = \frac{\mu(\Gamma)}{\mu_0} = [1 + (\lambda^*\Gamma^*)^2]^{(n-1)/2}. \tag{44b}$$

Hence, only two rheological parameters need to be fixed, which are $\lambda^* = \lambda\ell\|\nabla\mathscr{P}\|_{t=0}/\mu_{ref}$ and n. Following Airiau and Bottaro [38], the analysis is carried out fixing $\lambda^* = 5$ and $n = 0.5$.

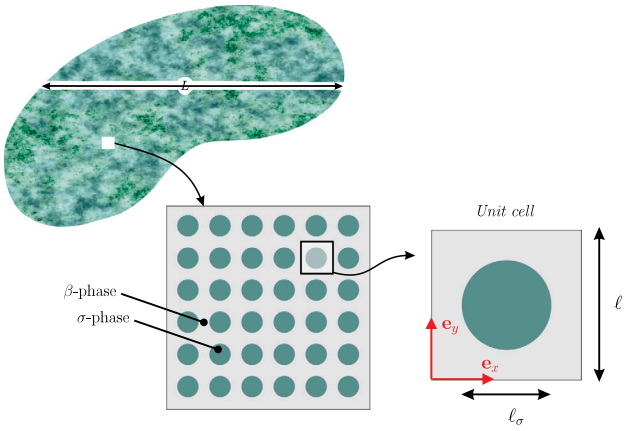

Fig. 2. Sketch of a periodic unit cell, of side length ℓ, for a model porous medium structure consisting of an array of inline cylinders of diameter ℓ_σ. $\mathbf{e}_x$ and $\mathbf{e}_y$ are the unit vectors in the horizontal and vertical directions, respectively.

6.2. Analysis for hydrostatic initial condition

As a first set of numerical experiments, consider the situation in which the fluid is initially at rest, *i.e.*, $\nabla\mathscr{P}_0 = \mathbf{0}$, so that $\mathbf{v}_0^* = \mathbf{0}$. In addition, let $\nabla^*\mathscr{P}^*$ be constant in time and equal to the expression given in Eq. (38). Under these conditions, $\boldsymbol{\alpha}_0^* = \mathbf{0}$ and $\mathbf{H}_\mu^*$ is a full tensor, whose components evolve over time.

The flow problem given in Eqs. (40) and the closure problem in Eqs. (41) were solved in the simple unit cell geometry depicted in Fig. 2, for $0 \leq \theta \leq 90°$, using the commercial finite element software Comsol Multiphysics 5.6. A direct solution scheme was employed making use of the PARDISO solver included in the software to numerically solve the initial flow, the unsteady flow and the closure problem. Through coupling solution steps, it was possible to save the dynamic information of the flow problem and use it in the closure problem solution. In addition, standard triangular mesh refinement techniques were used in order to ensure that the numerical solutions are independent of this numerical degree of freedom. It was found that using a dimensionless maximum element size of 0.025 for the fluid domain and of 0.01 at the boundaries, was sufficient in order to achieve mesh convergence.

In Fig. 3, the predictions of the dynamics of the components of the apparent permeability tensor are reported for creeping flow conditions ($Re \ll 1$) taking a porosity value of 0.9. Note that, under these conditions, $\mathbf{H}_\mu^*$ is symmetric. These transport conditions correspond to those studied by Airiau and Bottaro [38] for steady-state flow. The results are presented normalized by the xx-component of the dimensionless intrinsic permeability tensor (*i.e.*, K_{xx}^*), which is obtained by solving Eqs. (41) fixing $\mu(\Gamma) = \mu_{ref}$ under steady and non-inertial conditions. Clearly, the results from the work by Airiau and Bottaro [38] are retrieved for $t^* > 1$ for all values of θ, and this constitutes a first set of validation. As expected, the components of $\mathbf{H}_\mu^*$ start from zero and evolve over time until reaching a single steady-state value. Interestingly, the apparent permeability tensor is not spherical, despite the fact that the intrinsic permeability is indeed a spherical tensor, for this unit cell geometry. This is the consequence of the non-linear character of the Carreau model. Nevertheless, the off-diagonal components of the tensor are equal, which evidences that the tensor is symmetric as anticipated above. Note that the off-diagonal components start acquiring non-zero values at a time that is an order of magnitude larger than for their diagonal counterparts. Moreover, for this geometry, the off-diagonal components remain one order of magnitude smaller than the diagonal terms for the whole range of pressure gradient angles.

As a second case study, the predictions of the dynamics of the components of the apparent permeability tensor are reported for laminar flow ($Re = 1000$) in Fig. 4. The numerical simulations were

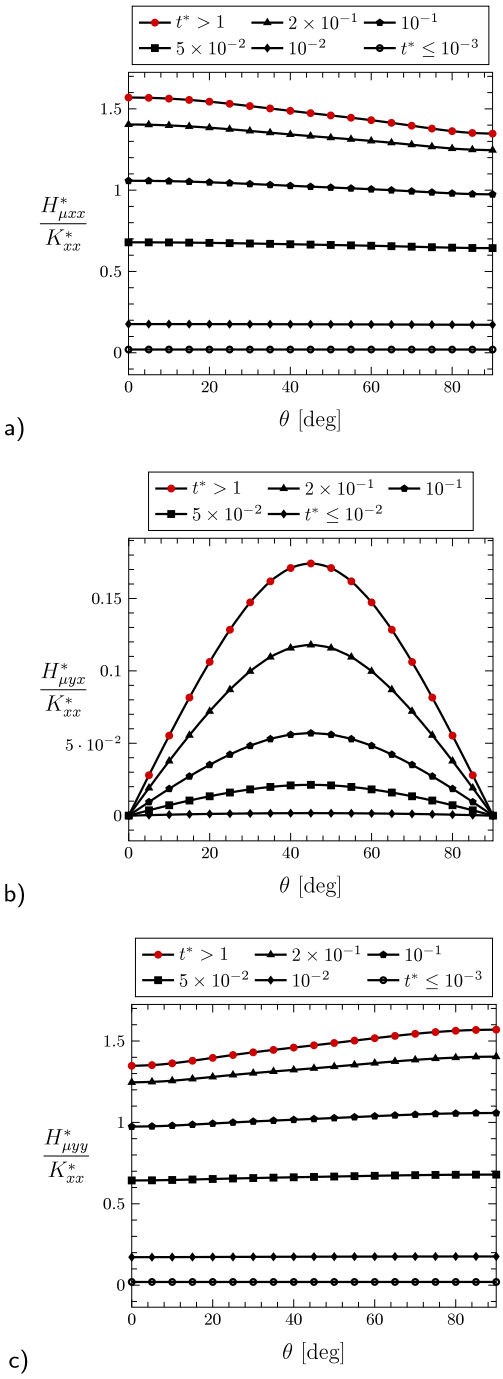

Fig. 3. Dynamics of the a) xx, b) yx and c) yy-components of the apparent permeability tensor (normalized by the xx-component of the intrinsic permeability tensor) under creeping flow conditions vs. the macroscopic pressure gradient angle θ for $\varepsilon = 0.9$. Red dots correspond to the values reported in figure 3b of Airiau and Bottaro [38].

performed in the same model structure used for $Re \ll 1$. As in Fig. 3, all the components of $\mathbf{H}_\mu^*$ increase over time, until reaching steady state for all angles. In contrast with the creeping flow regime, here, the apparent permeability tensor shows non-symmetrical properties, as expected. This is evidenced by the completely different values reported in Figs. 4b and 4c of the off-diagonal terms at all times. Moreover, the diagonally-opposite components of the tensor display specular values, *i.e.*, $H_{xx}(\theta) = H_{yy}(90°-\theta)$ (see Figs. 4a and 4d) and $H_{xy}(\theta) = H_{yx}(90°-\theta)$ (see Figs. 4b and 4c). This is a consequence of the orthotropic character of the unit cell. Also, in contrast to the creeping regime, the diagonal

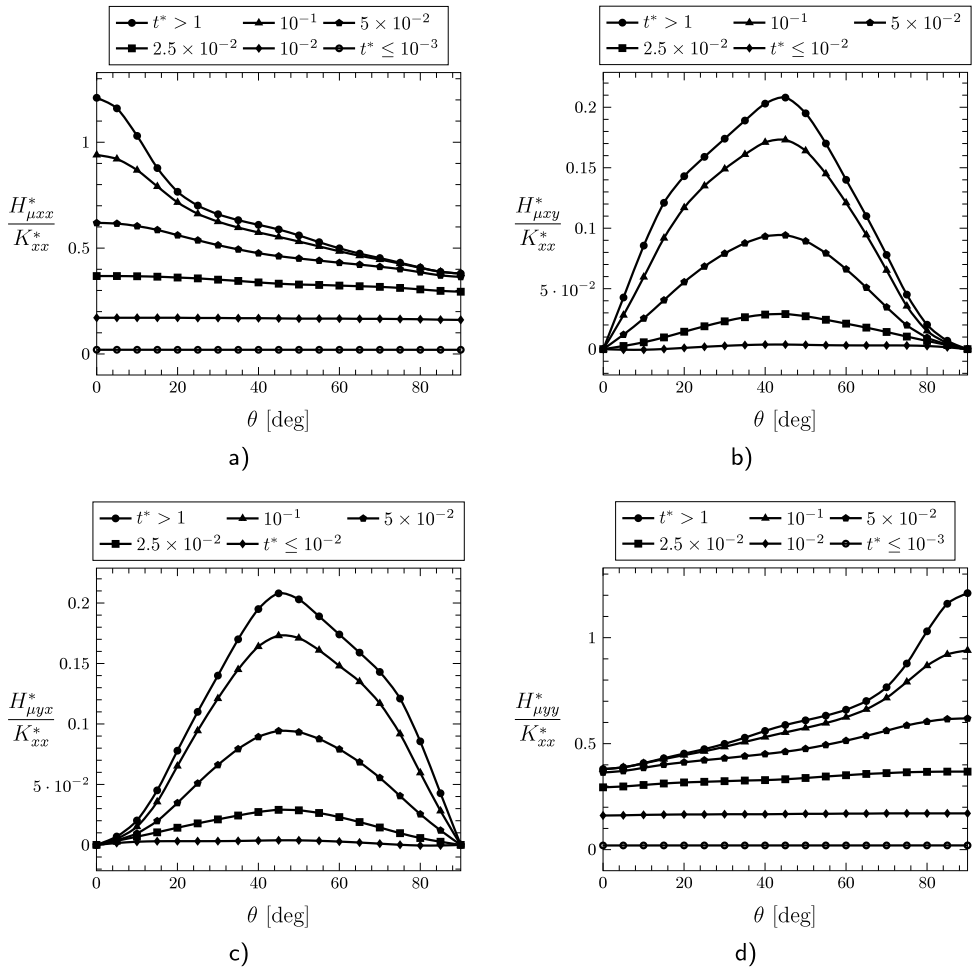

Fig. 4. Dynamics of the a) xx, b) yx, c) xy and d) yy-components of the apparent permeability tensor (normalized by the xx-component of the intrinsic permeability tensor) under laminar flow conditions ($Re = 1000$) vs. the macroscopic pressure gradient angle, θ, for $\varepsilon = 0.9$.

components exhibit important variations in magnitude with respect to the pressure gradient orientation while approaching steady state. This is attributed to the streamlines deformation induced by both inertia and viscous effects translating into a strong reduction of the values of the components of $\mathbf{H}_\mu$. In accordance with this, all components of the apparent permeability tensor are of the same order of magnitude for pressure gradient angles between 15° and 75°, despite the simplicity of the geometry under consideration. Furthermore, the off-diagonal components of the apparent permeability tensor exhibit a symmetry breakdown with respect to 45° over time. This symmetry breakdown is attributed to inertial effects, whose influence over the effective-medium coefficients are noticeable only after sufficient time has passed, as evidenced in figure 3 of [51]. This further indicates, as proved by the symmetry analysis, that under inertial non-Newtonian flow conditions, the non-symmetry of the tensor $\mathbf{H}^*_\mu$ is related to the physics regardless the geometry in the unit cell. This extends similar conclusions reached in the case of a Newtonian fluid [69].

6.3. Analysis for a non-zero initial flow condition

As a final case study, consider the situation in which the macroscopic pressure gradient has only one non-zero component in the horizontal direction and is time-dependent in an oscillatory manner according to the following expression

$$-\frac{d\mathscr{P}^*}{dx^*} = \begin{cases} -\frac{d\mathscr{P}^*_0}{dx^*} = 0.1, & t^* \leq 0, \\ -\frac{d\mathscr{P}^*_0}{dx^*} + 0.5\left(1 - \cos(\omega^* t^*)\right), & t^* > 0. \end{cases} \tag{45}$$

With this expression, it is meant that the initial flow results from a constant pressure gradient in the x-direction at $t = 0$, which is then oscillatory at $t > 0$. This particular form of the macroscopic pressure gradient has been used in previous works [51,52], and in the remainder of this section, the dimensionless frequency ω^* is set to 100 for the sake of brevity in the analysis, which could certainly be extended to other frequency values.

Since now the initial pressure gradient is non-zero, it is necessary to solve the initial flow problem in a unit cell, as given in Eqs. (37), in order to compute the field of $\mathbf{v}^*_0$. This solution is the initial condition of the flow problem defined in Eqs. (40), which is solved to obtain the dynamic dimensionless velocity field $\mathbf{v}^*$. Indeed, due to the nature of the macroscopic pressure gradient considered here, it is natural to expect that $\mathbf{v}^*$ is an oscillatory function of time that reaches a permanent, albeit unsteady state at sufficiently long times. Finally, the time-dependent velocity field is used in Eqs. (41) to compute the closure variable $\mathbf{F}^*$. With these elements available, it is possible to use Eqs. (42) to predict the effective-medium quantities $\mathbf{H}^*_\mu$ and $\boldsymbol{\alpha}^*_0$. Since the macroscopic pressure gradient is horizontal, corresponding to a symmetry axis of the unit cell, the macroscopic velocity is aligned with $\nabla^*\mathscr{P}^*$. Consequently, it is only necessary to compute the values of the xx-component of $\mathbf{H}^*_\mu$ and the x-component of $\boldsymbol{\alpha}^*_0$ in order to predict the horizontal component of the macroscale velocity vector as defined in Eq. (43).

In Fig. 5, the dynamics of $H^*_{\mu xx}$ and α^*_{0x} are reported for two Reynolds number values considering both non-Newtonian and Newtonian flow conditions. In the latter case, μ was taken equal to μ_0 (*i.e.,*

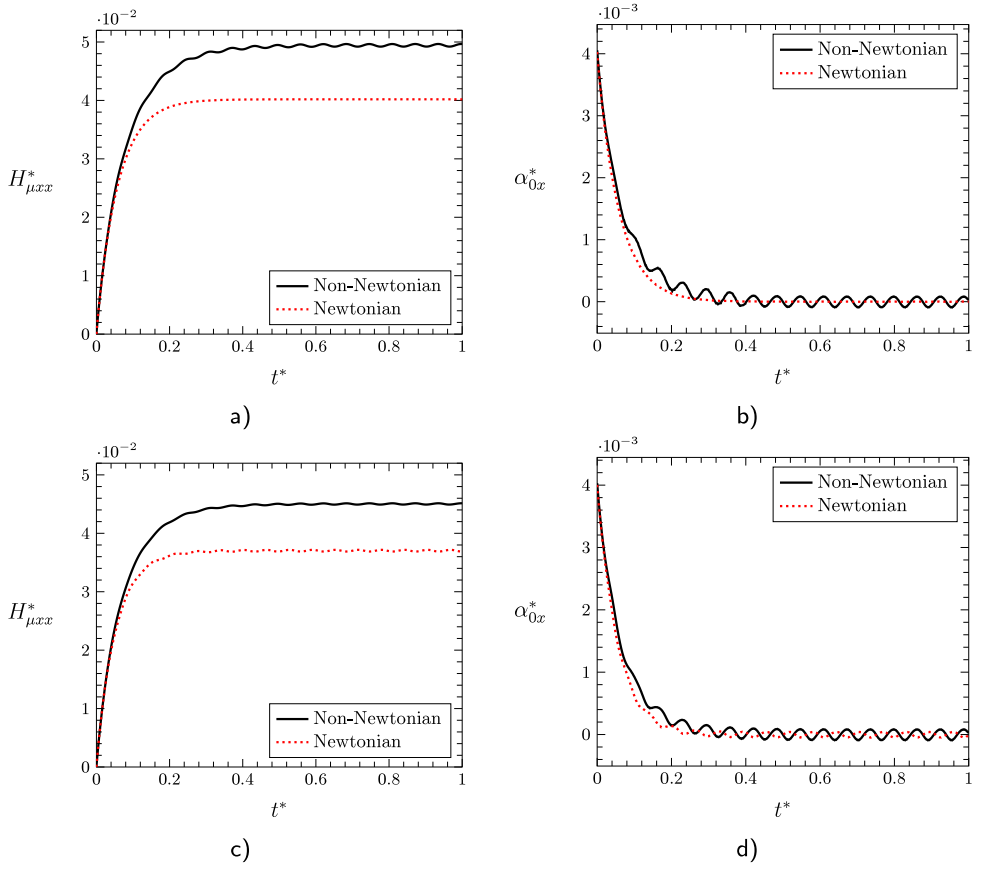

Fig. 5. Example of the Reynolds number influence on the dynamics of the dimensionless a), c) xx-component of the apparent permeability tensor ($H^*_{\mu xx}$) and b), d) the x-component of the memory vector α^*_{0x} for both non-Newtonian and Newtonian flows. Results in a) and b) correspond to $Re \leq 100$, whereas results in c) and d) are obtained for $Re = 10^3$. All the simulations result from solving the associated closure problem together with Eqs. (37) and (40) in the unit cell depicted in Fig. 2 for a porosity of 0.9.

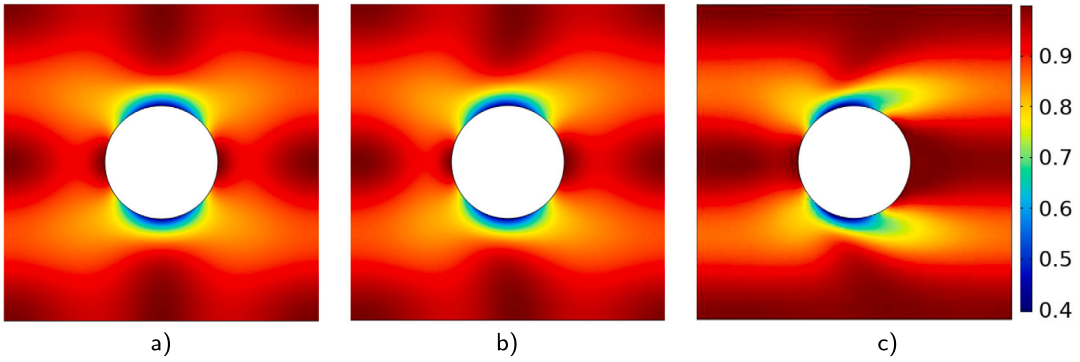

Fig. 6. Fields of $\mu(\Gamma^*)/\mu_{ref}$ at $t^* = 1$ corresponding to the simulations reported in Fig. 5 for a) $Re \ll 1$, b) $Re = 100$ and c) $Re = 1000$.

$\mu^* = 1$). These simulations were performed in the unit cell depicted in Fig. 2, taking a porosity value of 0.9. Regarding these results, the following comments are in order.

- Results on $H^*_{\mu xx}$ and α^*_{0x} are not noticeably modified when the Reynolds number is increased up to 100. Inertial effects remain weak in the interval $0 \leq Re \leq 100$ and do not significantly impact the field of $\mathbf{F}$ which is mainly viscosity-dependent. In particular, the local viscosity does not seem to be markedly affected by the convective acceleration in this range of Re. This is evidenced in the dimensionless viscosity field examples reported in Fig. 6 for $t^* = 1$ where no real contrast between the two fields at $Re \ll 1$ and $Re = 100$ is noticeable whereas a clear difference in the field of $\mu(\Gamma^*)/\mu_0$ is observable for $Re = 1000$. It must be noted that the apparent permeability is larger at any time in the non-Newtonian case. This is consistent with the fact that this coefficient is viscosity-dependent and the shear-thinning character of the fluid under consideration.
- The increase over time of $H^*_{\mu xx}$ (and the decrease over time of α^*_{0x}) does not allow distinguishing the non-Newtonian from the Newtonian flow case up until a threshold time, which is roughly equal to $t^*_0 \simeq 0.04$ in the configuration under study. This is to be expected since the closure problem initial condition is homogeneous for both non-Newtonian and Newtonian flows.
- For Reynolds number values smaller than or equal to 100, the results in Fig. 5a) show that the apparent permeability is oscillatory in the non-Newtonian case despite the vanishingly small influence of inertial effects. This is clearly the signature of the dependence of the viscosity on the velocity gradients and the impact of this

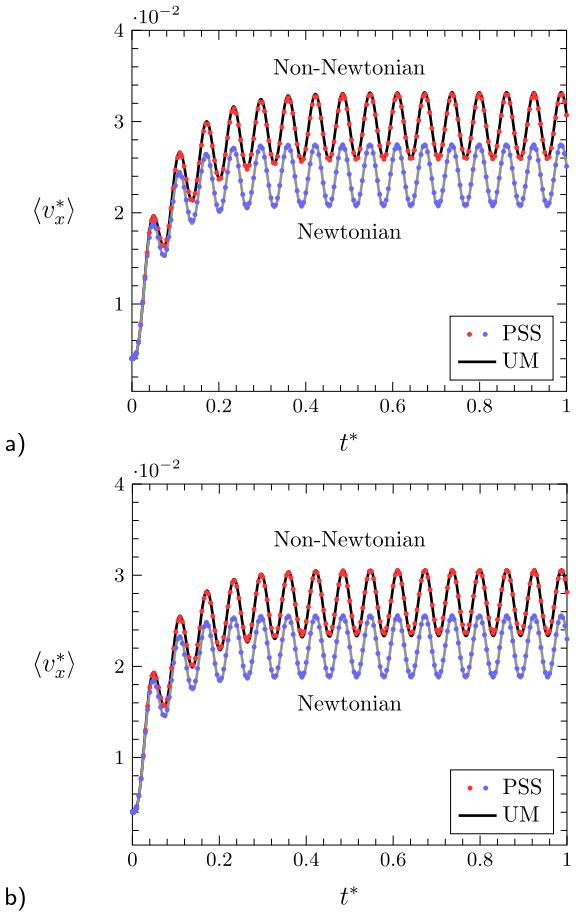

Fig. 7. Comparison of the predictions of the seepage velocity dynamics resulting from pore-scale simulations (PSS) and the upscaled model (UM) derived here. Results correspond to flow conditions reported in Fig. 5 taking a) $Re \leq 10^2$ and b) $Re = 10^3$.

interplay on the viscous term in a periodic unit cell. Conversely, in the Newtonian case no oscillations are observed, as expected, since the viscosity is constant in that case. These observations are also applicable to the results in Fig. 5b) for the dynamics of α_{0x}^*.

- As the Reynolds number increases, the amplitude of the apparent permeability oscillations in the non-Newtonian case are dampened but remain in phase compared to the case where inertia is insensitive. Dampening is clearly due to inertia, confirming that, in this range of Re, inertia and viscous effects are competing in the dynamics of the apparent permeability. Conversely, in the Newtonian case, inertia favors oscillations on the apparent permeability. Moreover, it should be noted that the oscillations are roughly out of phase with respect to the non-Newtonian case. Furthermore, for the memory term, α_{0x}^*, the oscillations in the permanent regime are practically the same (in amplitude and phase) for the two flow regimes considered here in the non-Newtonian case. This further illustrates the complex combined effects of inertia and viscosity in that case. As for the apparent permeability, oscillations are amplified by inertia in the Newtonian case and are out of phase compared to the non-Newtonian case. Note that in both situations, α_{0x}^* is centered on zero in the permanent regime. This is in agreement with the fact that, at sufficiently long time, the initial flow memory is lost.

With the above effective quantities at hand, it is now possible to provide predictions of the seepage velocity dynamics resulting from the upscaled model given in Eq. (43) and compare them with pore-scale simulations. The latter results from solving the flow problems given in Eqs. (37) and (40) in a horizontal array of unit cells, each one subject to the same macroscopic pressure gradient given in Eq. (45). The macroscopic velocity is then computed by taking the superficial average of the pore-scale velocity field over a unit cell positioned at the geometric center of the array. It is noted that an array of ten unit cells yields the same predictions as systems with larger sizes.

Results obtained by following this procedure are reported in Fig. 7 for both non-Newtonian and Newtonian flows. It may be noted from this figure that the characteristic time, t_0^*, corresponds to the oscillations onset of the macroscopic velocity. Moreover, the dynamics of the average velocities are perfectly in phase for both Newtonian and non-Newtonian flows. The velocity, in the latter case, is larger, at any time, than in the Newtonian case, the physical reason lying, as observed for the apparent permeabilities, in the shear-thinning character of the non-Newtonian flow. The comparison between pore-scale simulations and the predictions from the upscaled model show excellent agreement for both types of flows, proving that the upscaled model accurately reproduces the physics over time for the two Reynolds number values considered here. This serves as a validation of the model albeit this does not replace, by any means, the need for experimental validation. These simulations simply show that, as long as the assumptions that support the derivation of the upscaled model are met, the model performs satisfactorily.

The above results provide an illustrative application of the model derived here for a particular fluid flow (Carreau model) in a simple geometry. Undeniably, a variety of other generalized Newtonian fluid flows, porous media geometries and configurations could be investigated. However, this remains beyond the scope of the present work. Nevertheless, the same type of agreement with pore-scale simulations is expected for other types of non-Newtonian fluids and homogeneous media that comply with the constraints and assumptions involved in the upscaling process.

7. Discussion and conclusions

In this work, a macroscopic model for generalized Newtonian fluid flow under non-steady and inertial conditions in rigid and homogeneous porous media was derived considering an effective slip boundary condition at the solid–fluid interface. Since the analysis is restricted to incompressible flow and no mass transfer takes place between the fluid and solid phases, the upscaled mass conservation equation, obtained by making use of the classical volume averaging method, simply states that the seepage velocity is solenoidal. The macroscopic momentum transport equation resulted from a combination of a simplified version of the volume averaging method and the adjoint technique. The resulting expression has a Darcy-like structure that is non-local in time as it involves the convolution product between the temporal derivative of the apparent permeability tensor with the macroscopic pressure gradient. In addition, the macroscopic momentum balance equation incorporates a memory term of the initial condition. Both the apparent permeability tensor and the effective memory term are obtained from the solution of a single closure problem in a unit cell representative of the process. They depend on the magnitude and orientation of the macroscopic forcing. The apparent permeability tensor is not symmetric, in general, when inertia is present. However, it is symmetric in the creeping regime.

The model keeps a certain degree of generality as it can be used for any viscosity model that is compliant with generalized Newton's law. Indeed, the macroscopic model structure is identical to the one reported for Newtonian flow [51–53]. In addition, under creeping steady-state conditions and no slip effect at the solid–fluid interface, the model reduces to that reported in [38]. Numerical results of the components of the apparent permeability tensor under unsteady conditions, and for a simple 2D model structure, are in agreement with those reported in this reference after reaching steady state. Moreover, the dynamics of the apparent permeability components were shown to be quite sensitive to the flow regime. In fact, the off-diagonal components of the apparent

permeability tensor yield a contribution to the flow of comparable importance with respect to their diagonal counterparts for almost all the macroscopic pressure gradient orientations under consideration.

The performance of the model to predict the flow dynamics was validated by comparison of the seepage velocity with the results from pore-scale simulations in a simple periodic representation of the porous medium structure considering an oscillatory macroscopic pressure gradient. Excellent agreement was found between the two approaches. Contrary to the Newtonian case, the apparent permeability is influenced by the oscillatory nature of the forcing, even under creeping flow conditions, during the permanent regime. The numerical validation achieved in this work does not replace comparison with experimental results and calls upon more experimental test of non-Newtonian flow in porous media in various conditions.

It must be emphasized that the validations reported here do not cover all the degrees of freedom presented in the model. For instance, a detailed analysis of the effect of geometrical anisotropy, its interaction with the fluid rheology and the resulting effective-medium quantities is certainly interesting. Nevertheless, the model performance should not be compromised by the unit cell geometry, since no assumption is made regarding this feature in the derivations. Another point of discussion is the interfacial slip. Again, since no particular assumptions were made during the upscaling process, while employing this condition, there is no reason to doubt about the predictive capabilities of the model in this regard as it was investigated in the Newtonian case (see, for example, [52]). Nevertheless, for the non-Newtonian case, it would be interesting to investigate the impact of slip on the effective-medium quantities. However, such an analysis must only be made within the range of validity of the slip boundary condition. These investigations deserve a more exhaustive set of simulations and will be addressed in a future work.

Finally, the model derived here is a generalization of previous approaches, showing the versatility of the upscaling method used in this work. Extensions to other flow and transport situations are certainly desirable and will be the subject of future investigations.

Declaration of competing interest

The authors declare that they have no known competing financial interests or personal relationships that could have appeared to influence the work reported in this paper.

Data availability

Data will be made available on request.

Acknowledgment

Sánchez-Vargas is thankful to Consejo Nacional de Ciencia *y* Tecnología (CONACYT), Mexico for providing her PhD scholarship (No. 802319).

Appendix A. Green's formulas

In this appendix, proofs of Green's formulas given in Eqs. (12a), (12b) and (12c) are provided. To begin with, attention is focused on Eq. (12a).

The starting point is Green's formula given in equation (A1) of Appendix A in [52], which can be written in an alternative form as

$$\begin{aligned}&\int_{\mathscr{V}_\beta}\left[\mathbf{a}\cdot\left(\nabla\cdot\left(c\left(\nabla\mathbf{B}+\nabla\mathbf{B}^{T1}\right)\right)\right)\right.\\&\qquad\left.-\left(\nabla\cdot\left(c\left(\nabla\mathbf{a}+\nabla\mathbf{a}^{T}\right)\right)\right)\cdot\mathbf{B}\right]\,dV\\&=\int_{\mathscr{A}_\beta}\left[\mathbf{a}\cdot\left(\mathbf{n}\cdot c\left(\nabla\mathbf{B}+\nabla\mathbf{B}^{T1}\right)\right)\right.\\&\qquad\left.-\mathbf{n}\cdot c\left(\nabla\mathbf{a}+\nabla\mathbf{a}^{T}\right)\cdot\mathbf{B}\right]\,dA.\end{aligned}\tag{A.1}$$

The procedure to reach this expression is the same as in the cited reference, in which, however, $\mathbf{u}$ is identified to $\mathbf{a}$, $\mathbf{W}$ to $c\left(\nabla\mathbf{B}+\nabla\mathbf{B}^{T1}\right)$ in equation (A2a), $\mathbf{U}$ to $c\left(\nabla\mathbf{a}+\nabla\mathbf{a}^{T}\right)$ and $\mathbf{V}$ to $\mathbf{B}$ in equation (A2b). In addition, the fact that $\mathbf{n}\cdot\left[\mathbf{a}\cdot c\left(\nabla\mathbf{B}+\nabla\mathbf{B}^{T1}\right)\right]=\mathbf{a}\cdot\left[\mathbf{n}\cdot c\left(\nabla\mathbf{B}+\nabla\mathbf{B}^{T1}\right)\right]$ was taken into account.

Next, consider the identity

$$\begin{aligned}\nabla\cdot(\mathbf{ca}\cdot\mathbf{B})&=\nabla\cdot(\mathbf{ca})\cdot\mathbf{B}+(\mathbf{ca})^{T}\,:\,\nabla\mathbf{B}\\&=(\nabla\cdot\mathbf{ca}+\mathbf{c}\cdot\nabla\mathbf{a})\cdot\mathbf{B}+\mathbf{a}\cdot(\mathbf{c}\cdot\nabla\mathbf{B}).\end{aligned}\tag{A.2a}$$

Upon integration over $\mathscr{V}_\beta$, and making use of the divergence theorem, it gives

$$\begin{aligned}&\int_{\mathscr{V}_\beta}\left[\mathbf{a}\cdot(\mathbf{c}\cdot\nabla\mathbf{B})+\mathbf{c}\cdot\nabla\mathbf{a}\cdot\mathbf{B}+\nabla\cdot\mathbf{ca}\cdot\mathbf{B}\right]\,dV=\\&\int_{\mathscr{A}_\beta}\mathbf{n}\cdot\mathbf{ca}\cdot\mathbf{B}\,dA.\end{aligned}\tag{A.2b}$$

Additionally, the following identities can be considered

$$\nabla\cdot(\mathbf{ab})=\nabla\cdot\mathbf{ab}+\mathbf{a}\cdot\nabla\mathbf{b},\tag{A.3a}$$

$$\nabla\cdot(a\mathbf{B})=\nabla a\cdot\mathbf{B}+a\nabla\cdot\mathbf{B},\tag{A.3b}$$

and can also be integrated over $\mathscr{V}_\beta$, which, by making use of the divergence theorem, yield

$$\begin{aligned}\int_{\mathscr{V}_\beta}(\nabla\cdot\mathbf{ab}+\mathbf{a}\cdot\nabla\mathbf{b})\,dV&=\int_{\mathscr{A}_\beta}\mathbf{n}\cdot\mathbf{ab}\,dA\\&=\int_{\mathscr{A}_\beta}\mathbf{a}\cdot\left[\mathbf{n}\cdot(\mathbf{lb})\right]\,dA,\end{aligned}\tag{A.3c}$$

$$\begin{aligned}\int_{\mathscr{V}_\beta}(\nabla a\cdot\mathbf{B}+a\nabla\cdot\mathbf{B})\,dV&=\int_{\mathscr{A}_\beta}\mathbf{n}\cdot a\mathbf{B}\,dA\\&=\int_{\mathscr{A}_\beta}\mathbf{n}\cdot(\mathbf{l}a)\cdot\mathbf{B}\,dA.\end{aligned}\tag{A.3d}$$

Adding Eqs. (A.1), (A.2b) and (A.3d) pre-multiplied by a constant d, and finally subtracting Eq. (A.3c) to the resulting expression leads to

$$\begin{aligned}&\int_{\mathscr{V}_\beta}\left[\mathbf{a}\cdot\left(d\mathbf{c}\cdot\nabla\mathbf{B}-\nabla\mathbf{b}+\nabla\cdot\left[c\left(\nabla\mathbf{B}+\nabla\mathbf{B}^{T1}\right)\right]\right)\right.\\&\qquad\left.-\left(-d\mathbf{c}\cdot\nabla\mathbf{a}-\nabla a+\nabla\cdot\left[c\left(\nabla\mathbf{a}+\nabla\mathbf{a}^{T}\right)\right]\right)\cdot\mathbf{B}\right]\,dV\\&-\int_{\mathscr{V}_\beta}(\nabla\cdot\mathbf{ab}-d\nabla\cdot\mathbf{ca}\cdot\mathbf{B}-a\nabla\cdot\mathbf{B})\,dV\\&=\int_{\mathscr{A}_\beta}\left[\mathbf{a}\cdot\left(\mathbf{n}\cdot\left(-\mathbf{lb}+c(\nabla\mathbf{B}+\nabla\mathbf{B}^{T1})\right)\right)\right.\\&\qquad\left.-\mathbf{n}\cdot\left(-d\mathbf{ca}-\mathbf{l}a+c\left(\nabla\mathbf{a}+\nabla\mathbf{a}^{T}\right)\right)\cdot\mathbf{B}\right]\,dA,\end{aligned}\tag{A.4}$$

which is Eq. (12a), hence completing the proof of this Green's formula.

To demonstrate the formula in Eq. (12b), it is convenient to consider the above result and form the left dyadic product of this equality by a constant arbitrary vector, denoted $\boldsymbol{\lambda}$. Keeping in mind that $\boldsymbol{\lambda}$ is indeed constant, the following identities are to be considered

$$\boldsymbol{\lambda}\mathbf{c}\cdot\nabla\mathbf{a}=(\mathbf{c}\cdot\nabla\mathbf{a}\boldsymbol{\lambda})^{T}=(\mathbf{c}\cdot\nabla(\mathbf{a}\boldsymbol{\lambda}))^{T},\tag{A.5a}$$

$$\boldsymbol{\lambda}\nabla a=(\nabla a\boldsymbol{\lambda})^{T}=(\nabla(a\boldsymbol{\lambda}))^{T},\tag{A.5b}$$

$$\begin{aligned}\boldsymbol{\lambda}\nabla\cdot\left(\nabla\mathbf{a}+\nabla\mathbf{a}^{T}\right)&=\left(\nabla\cdot\left(\nabla\mathbf{a}+\nabla\mathbf{a}^{T}\right)\boldsymbol{\lambda}\right)^{T}\\&=\left(\nabla\cdot\left(\nabla(\mathbf{a}\boldsymbol{\lambda})+(\nabla(\mathbf{a}\boldsymbol{\lambda}))^{T1}\right)\right)^{T},\end{aligned}\tag{A.5c}$$

$$\boldsymbol{\lambda}\nabla\cdot\mathbf{ab}=\nabla\cdot(\mathbf{a}\boldsymbol{\lambda})\mathbf{b},\tag{A.5d}$$

$$\boldsymbol{\lambda}\mathbf{n}\cdot\mathbf{ca}=\mathbf{n}\cdot\mathbf{c}\boldsymbol{\lambda}\mathbf{a}=(\mathbf{n}\cdot\mathbf{ca}\boldsymbol{\lambda})^{T},\tag{A.5e}$$

$$\boldsymbol{\lambda}\mathbf{n}a=(\mathbf{n}\boldsymbol{\lambda}a)^{T},\tag{A.5f}$$

$$\begin{aligned}\boldsymbol{\lambda}\mathbf{n}\cdot\left(\nabla\mathbf{a}+\nabla\mathbf{a}^{T}\right)&=\left(\mathbf{n}\cdot\left(\nabla\mathbf{a}+\nabla\mathbf{a}^{T}\right)\boldsymbol{\lambda}\right)^{T}\\&=\left(\mathbf{n}\cdot\left(\nabla(\mathbf{a}\boldsymbol{\lambda})+(\nabla(\mathbf{a}\boldsymbol{\lambda}))^{T1}\right)\right)^{T}.\end{aligned}\tag{A.5g}$$

Once these identities are used in the outer product between λ and Eq. (A.4), and after identifying $\mathbf{a}\lambda \equiv \mathbf{A}$ and $a\lambda \equiv \mathbf{a}$, the following result is obtained

$$\begin{aligned}
&\int_{\mathscr{V}_\beta} \Big[\mathbf{A}^T \cdot \left(d\mathbf{c}\cdot\nabla\mathbf{B} - \nabla\mathbf{b} + \nabla\cdot\left[c\left(\nabla\mathbf{B}+\nabla\mathbf{B}^{T1}\right)\right]\right) \\
&\quad - \left(-d\mathbf{c}\cdot\nabla\mathbf{A} - \nabla\mathbf{a} + \nabla\cdot\left[c\left(\nabla\mathbf{A}+\nabla\mathbf{A}^{T1}\right)\right]\right)^T \cdot \mathbf{B}\Big]\, dV \\
&+ \int_{\mathscr{V}_\beta} \left(d\nabla\cdot\mathbf{c}\mathbf{A}^T\cdot\mathbf{B} - \nabla\cdot\mathbf{A}\mathbf{b} + \mathbf{a}\nabla\cdot\mathbf{B}\right)\, dV \\
&= \int_{\mathscr{A}_\beta} \Big[\mathbf{A}^T\cdot\left(\mathbf{n}\cdot\left(-\mathbf{l}\mathbf{b} + c\left(\nabla\mathbf{B}+\nabla\mathbf{B}^{T1}\right)\right)\right) \\
&- \left(\mathbf{n}\cdot\left(-d\mathbf{c}\mathbf{A} - \mathbf{l}\mathbf{a} + c\left(\nabla\mathbf{A}+\nabla\mathbf{A}^{T1}\right)\right)\right)^T\cdot\mathbf{B}\Big]\, dA,
\end{aligned} \tag{A.6}$$

which corresponds to Green's formula given in Eq. (12b), hence completing its proof.

Turning the attention to Eq. (12c), it is convenient to use the substitutions $\mathbf{B} = \mathbf{b}\lambda$ and $\mathbf{b} = b\lambda$, considering λ as a constant arbitrary unit vector, and introduce them into the formula given in Eq. (A.4). Once this is done and the right inner product of the result is formed with λ, the following relationship is obtained

$$\begin{aligned}
&\int_{\mathscr{V}_\beta} \Big[\mathbf{a}\cdot\left(d\mathbf{c}\cdot\nabla\mathbf{b} - \nabla b + \nabla\cdot c\left(\nabla\mathbf{b}+\nabla\mathbf{b}^T\right)\right) \\
&\quad - \left(-d\mathbf{c}\cdot\nabla\mathbf{a} - \nabla a + \nabla\cdot c\left(\nabla\mathbf{a}+\nabla\mathbf{a}^T\right)\right)\cdot\mathbf{b}\Big]\, dV \\
&- \int_{\mathscr{V}_\beta} \left(b\nabla\cdot\mathbf{a} - d\nabla\cdot\mathbf{c}\mathbf{a}\cdot\mathbf{b} - a\nabla\cdot\mathbf{b}\right)\, dV \\
&= \int_{\mathscr{A}_\beta} \Big[\mathbf{a}\cdot\left(\mathbf{n}\cdot\left(d\mathbf{c}\mathbf{b} - \mathbf{l}b + c\left(\nabla\mathbf{b}+\nabla\mathbf{b}^T\right)\right)\right) \\
&\quad - \left(\mathbf{n}\cdot\left(-\mathbf{l}a + c\left(\nabla\mathbf{a}+\nabla\mathbf{a}^T\right)\right)\right)\cdot\mathbf{b}\Big]\, dA,
\end{aligned} \tag{A.7}$$

which is Green's formula given in Eq. (12c), thus concluding the proof.

Appendix B. Fluid pressure deviations solution in the Laplace domain

The purpose of this appendix is the derivation of a formal solution for $\hat{p}$ by making use of Green's formulas in a way similar to that adopted to obtain $\hat{\mathbf{v}}$ in Section 4. To this end, let the adjoint Green's function pair for the fluid pressure deviations in the Laplace domain be $\hat{g}_a$ and $\hat{\mathbf{g}}_p$. They are the solution of the following boundary-value problem

$$\nabla\cdot\hat{\mathbf{g}}_p = \delta(\mathbf{r}-\mathbf{r}_0) - \frac{1}{V_\beta}, \quad \text{in } \mathscr{V}_\beta, \tag{B.1a}$$

$$\begin{aligned}
&\boldsymbol{\beta} + \rho s\hat{\mathbf{g}}_p - \rho\mathbf{v}_\Delta\cdot\nabla\hat{\mathbf{g}}_p = -\nabla\hat{g}_a \\
&\qquad + \nabla\cdot\left[\mu(\Gamma_\Delta)\left(\nabla\hat{\mathbf{g}}_p + \nabla\hat{\mathbf{g}}_p^T\right)\right], \quad \text{in } \mathscr{V}_\beta,
\end{aligned} \tag{B.1b}$$

$$\hat{\mathbf{g}}_p = -S_\Delta\mathbf{P}\cdot\left(\mathbf{n}\cdot\left(\nabla\hat{\mathbf{g}}_p + \nabla\hat{\mathbf{g}}_p^T\right)\right), \quad \text{at } \mathscr{A}_{\beta\sigma}, \tag{B.1c}$$

$$\psi(\mathbf{r}+\mathbf{l}_i) = \psi(\mathbf{r}), \quad i = 1,2,3;\ \psi = \hat{\mathbf{g}}_p, \hat{g}_a, \tag{B.1d}$$

$$\hat{g}_a = 0, \quad \text{at } \mathbf{r} = \mathbf{r}_a. \tag{B.1e}$$

In equation Eq. (B.1b), $\boldsymbol{\beta}$ is a function of $\mathbf{r}$. In order to find the relationship between these Green's functions and the pressure deviations, Green's formula in the form given in Eq. (12c) can be used. Setting $a = \hat{\tilde{p}}$, $\mathbf{a} = \hat{\mathbf{v}}$, $\mathbf{c} = \mathbf{v}_\Delta$, $b = \hat{g}_a$, $\mathbf{b} = \hat{\mathbf{g}}_p$, $c = \mu(\Gamma_\Delta)$ and $d = \rho$, and taking into account that $\hat{\mathbf{v}}$ and $\mathbf{v}_\Delta$ are solenoidal fields, along with periodicity that allows reducing the area integral to $\mathscr{A}_{\beta\sigma}$ only, it results that

$$\begin{aligned}
&\int_{\mathscr{V}_\beta} \Big[\hat{\mathbf{v}}\cdot\left(\rho\mathbf{v}_\Delta\cdot\nabla\hat{\mathbf{g}}_p - \nabla\hat{g}_a + \nabla\cdot\mu(\Gamma_\Delta)\left(\nabla\hat{\mathbf{g}}_p+\nabla\hat{\mathbf{g}}_p^T\right)\right) \\
&\quad - \hat{\mathbf{g}}_p\cdot\left(-\rho\mathbf{v}_\Delta\cdot\nabla\hat{\mathbf{v}} - \nabla\hat{\tilde{p}} + \nabla\cdot\mu(\Gamma_\Delta)\left(\nabla\hat{\mathbf{v}}+\nabla\hat{\mathbf{v}}^T\right)\right)\Big]\, dV \\
&+ \int_{\mathscr{V}_\beta} \nabla\cdot\hat{\mathbf{g}}_p\hat{\tilde{p}}\, dV = \int_{\mathscr{A}_{\beta\sigma}} \mathbf{n}\cdot\left[\mathbf{v}_\Delta\rho\hat{\mathbf{v}}\cdot\hat{\mathbf{g}}_p - \hat{\mathbf{v}}\hat{g}_a + \hat{\mathbf{g}}_p\hat{\tilde{p}}\right]\, dA \\
&+ \int_{\mathscr{A}_{\beta\sigma}} \mu\left(\Gamma_\Delta\right)\mathbf{n}\cdot\Big[\left(\nabla\hat{\mathbf{g}}_p + \nabla\hat{\mathbf{g}}_p^T\right)\cdot\hat{\mathbf{v}} \\
&\quad - \left(\nabla\hat{\mathbf{v}} + \nabla\hat{\mathbf{v}}^T\right)\cdot\hat{\mathbf{g}}_p\Big]\, dA.
\end{aligned} \tag{B.2}$$

The first area integral term on the right-hand side of this relationship is zero due to the tangential character of $\mathbf{v}_\Delta$, $\hat{\mathbf{v}}$ and $\hat{\mathbf{g}}_p$ at $\mathscr{A}_{\beta\sigma}$. In addition, substituting the boundary conditions for $\hat{\mathbf{v}}$ and $\hat{\mathbf{g}}_p$ given in Eqs. (16c) and (B.1c) into the second interfacial term, and using the nomenclature $\mathbf{A} \equiv \nabla\hat{\mathbf{g}}_p + \nabla\hat{\mathbf{g}}_p$ and $\mathbf{B} \equiv \nabla\hat{\mathbf{v}} + \nabla\hat{\mathbf{v}}^T$ yields

$$\begin{aligned}
&\int_{\mathscr{A}_{\beta\sigma}} \mu\left(\Gamma_\Delta\right)\mathbf{n}\cdot\left[\mathbf{A}\cdot\hat{\mathbf{v}} - \mathbf{A}\cdot\hat{\mathbf{g}}_p\right]\, dA = \\
&- \int_{\mathscr{A}_{\beta\sigma}} \mu\left(\Gamma_\Delta\right) S_\Delta\big[\mathbf{n}\cdot\mathbf{A}\cdot\mathbf{P}\cdot(\mathbf{n}\cdot\mathbf{B}) \\
&\qquad - \mathbf{n}\cdot\mathbf{B}\cdot\mathbf{P}\cdot(\mathbf{n}\cdot\mathbf{A})\big]\, dA.
\end{aligned} \tag{B.3}$$

Since $\mathbf{P}$ is a symmetric tensor, the first term inside the integral on the right-hand side of this last expression can equivalently be written as $\mathbf{n}\cdot\mathbf{A}\cdot\mathbf{P}\cdot(\mathbf{n}\cdot\mathbf{B}) = \mathbf{P}\cdot(\mathbf{n}\cdot\mathbf{A})\cdot(\mathbf{n}\cdot\mathbf{B}) = \mathbf{n}\cdot\mathbf{B}\cdot\mathbf{P}\cdot(\mathbf{n}\cdot\mathbf{A})$. This proves that the second area integral term on the right-hand side of Eq. (B.2) is also zero. Substitution of the corresponding expressions extracted from the momentum-like Eqs. (16b) and (B.1b) in the remaining volume integral term of Eq. (B.2) leads to

$$\hat{\tilde{p}} = \int_{\mathscr{V}_\beta} \hat{\mathbf{g}}_p\, dV\cdot\left(\nabla\langle\hat{p}\rangle^\beta - \frac{\rho}{s}\mathbf{g}\right) - \rho\int_{\mathscr{V}_\beta}\hat{\mathbf{g}}_p\cdot\mathbf{v}_0\, dV + \hat{\varphi}. \tag{B.4}$$

In the above equation $\hat{\varphi}$ is a constant in space. As a final step, it is now of interest to determine the relationship between the adjoint Green's function pair for the pressure and the Green's function pair $(\mathbf{G}_v, \mathbf{g}_v)$ for the velocity in the Laplace domain. To this end, consider the expression of Green's formula given in Eq. (12a). Setting, $a = \hat{g}_a$, $\mathbf{a} = \hat{\mathbf{g}}_p$, $\mathbf{c} = \mathbf{v}_\Delta$, $\mathbf{b} = \hat{\mathbf{g}}_v$, $\mathbf{B} = \hat{\mathbf{G}}_v$, $c = \mu(\Gamma_\Delta)$ and $d = -\rho$, taking into account that $\mathbf{v}_\Delta$ and $\hat{\mathbf{G}}_v$ are divergence-free fields, as well as the periodicity condition that allows reducing the area integral to $\mathscr{A}_{\beta\sigma}$, this formula takes the following expression

$$\begin{aligned}
&\int_{\mathscr{V}_\beta} \Big[\hat{\mathbf{g}}_p\cdot\Big(-\rho\mathbf{v}_\Delta\cdot\nabla\hat{\mathbf{G}}_v - \nabla\hat{\mathbf{g}}_v \\
&\qquad + \nabla\cdot\left[\mu(\Gamma_\Delta)\left(\nabla\hat{\mathbf{G}}_v + \nabla\hat{\mathbf{G}}_v^{T1}\right)\right]\Big) - \Big(\rho\mathbf{v}_\Delta\cdot\nabla\hat{\mathbf{g}}_p - \nabla\hat{g}_a \\
&\qquad + \nabla\cdot\left[\mu(\Gamma_\Delta)\left(\nabla\hat{\mathbf{g}}_p + \nabla\hat{\mathbf{g}}_p^T\right)\right]\Big)\cdot\hat{\mathbf{G}}_v\Big]\, dV \\
&- \int_{\mathscr{V}_\beta} \nabla\cdot\hat{\mathbf{g}}_p\hat{\mathbf{g}}_v\, dV \\
&= \int_{\mathscr{A}_{\beta\sigma}} \mathbf{n}\cdot\left(\hat{\mathbf{g}}_p\hat{\mathbf{g}}_v - \rho\mathbf{v}_\Delta\hat{\mathbf{g}}_p\cdot\hat{\mathbf{G}}_v + \hat{g}_a\hat{\mathbf{G}}_v\right)\, dA \\
&+ \int_{\mathscr{A}_{\beta\sigma}} \mu\left(\Gamma_\Delta\right)\mathbf{n}\cdot\Big[\hat{\mathbf{g}}_p\cdot\left(\nabla\hat{\mathbf{G}}_v + \nabla\hat{\mathbf{G}}_v^{T1}\right) \\
&\qquad - \left(\nabla\hat{\mathbf{g}}_p + \nabla\hat{\mathbf{g}}_p^T\right)\cdot\hat{\mathbf{G}}_v\Big]\, dA.
\end{aligned} \tag{B.5}$$

Because $\hat{\mathbf{g}}_p$, $\mathbf{v}_\Delta$ and $\hat{\mathbf{G}}_v$ are all tangential at $\mathscr{A}_{\beta\sigma}$, the first area integral term on the right-hand side of the above expression is zero. Moreover, once the expressions of $\hat{\mathbf{g}}_p$ and $\hat{\mathbf{G}}_v$ at the solid–fluid interface given in Eqs. (21c) and (B.1c) are considered, and following the development reported in Appendix A in [52], the second area integral term is also zero. After substitution of the corresponding expressions taken from the momentum-like Eqs. (21b) and (B.1b) into the volume integral terms on the left-hand side, and after some algebraic steps, the following result is obtained

$$\hat{\mathbf{g}}_p = -\hat{\mathbf{g}}_v. \tag{B.6}$$

Substitution of this expression into Eq. (B.4) leads to Eq. (25b).

Appendix C. Symmetry and positiveness of $\mathbf{H}_\mu$

In this appendix, symmetry and positiveness of the apparent permeability tensor, $\mathbf{H}_\mu$, are analyzed, following the same steps as in [51] (section 3.3) and [52] (Appendix C).

Forming the left dot product of Eq. (27b) with $s\hat{\mathbf{F}}$ and applying the superficial averaging operator to the result, while taking into account the solenoidal nature of $\hat{\mathbf{F}}$ and periodicity, yields

$$\hat{\mathbf{H}}_\mu^T = \frac{\rho}{\mu_{ref}} s^2 \left\langle \hat{\mathbf{F}}^T \cdot \hat{\mathbf{F}} \right\rangle + \frac{\rho}{\mu_{ref}} s \left\langle \hat{\mathbf{F}}^T \cdot \left(\mathbf{v}_\Delta \cdot \nabla \hat{\mathbf{F}} \right) \right\rangle - s \left\langle \hat{\mathbf{F}}^T \cdot \left[\nabla \cdot \left(\frac{\mu}{\mu_{ref}} \left(\nabla \hat{\mathbf{F}} + \nabla \hat{\mathbf{F}}^{T1} \right) \right) \right] \right\rangle. \tag{C.1}$$

The first term on the right-hand side of the above equation is symmetric, whereas the second one is skew-symmetric (see the proof in [66], section II.A). Moreover, using the nomenclature $\hat{\mathbf{B}} = \frac{\mu}{\mu_{ref}} \left(\nabla \hat{\mathbf{F}} + \nabla \hat{\mathbf{F}}^{T1} \right)$, the third term (divided by s) can be equivalently rewritten as (see corresponding algebraic steps in [52], Appendix C)

$$\left\langle \hat{\mathbf{F}}^T \cdot \left(\nabla \cdot \hat{\mathbf{B}} \right) \right\rangle = - \left\langle \nabla \hat{\mathbf{F}}^{T3} : \hat{\mathbf{B}} \right\rangle - \int_{\mathscr{A}_{\beta\sigma}} S_\Delta \frac{\mu_{ref}}{\mu} \mathbf{A} \cdot \mathbf{A}^T \, dA, \tag{C.2}$$

where $\mathbf{A} = \mathbf{n} \cdot \hat{\mathbf{B}}^{T2} \cdot \mathbf{P}$ and : is the double dot product in the nested convention sense. Here, the superscripts $T2$ and $T3$ respectively denote the transposes defined as $B^{T2}_{ijk} = B_{ikj}$ and $B^{T3}_{ijk} = B_{kji}$. The last term on the right-hand side of this last expression is obviously symmetric. Moreover, it can be shown (see [52], Appendix C) that the first is also a symmetric tensor. Consequently, it can be deduced that Eq. (C.1) performs a decomposition of $\hat{\mathbf{H}}_\mu$ in its principal parts showing that this tensor is not symmetric, in general, and that the skew symmetric part originates from inertial effects only. Since the Laplace transform does not alter symmetry properties, the same conclusions apply to $\mathbf{H}_\mu$.

At this point, positiveness can be analyzed, and to do so, it is convenient to substitute Eq. (C.2) into Eq. (C.1) and add the result to its transpose to obtain

$$\frac{1}{2} \left(\hat{\mathbf{H}}_\mu + \hat{\mathbf{H}}_\mu^T \right) = \frac{\rho}{\mu_{ref}} s^2 \left\langle \hat{\mathbf{F}}^T \cdot \hat{\mathbf{F}} \right\rangle + s \left\langle \nabla \hat{\mathbf{F}}^{T3} : \hat{\mathbf{B}} \right\rangle + s \int_{\mathscr{A}_{\beta\sigma}} S_\Delta \frac{\mu_{ref}}{\mu} \mathbf{A} \cdot \mathbf{A}^T \, dA. \tag{C.3}$$

Forming the left and right dot products of this equation with an arbitrary constant vector, λ, and following steps reported in [51] (equations (3.25) to (3.29)), leads to

$$\lambda \cdot \hat{\mathbf{H}}_\mu \cdot \lambda = \frac{\rho}{\mu_{ref}} s^2 \left\langle \left(\hat{\mathbf{F}} \cdot \lambda \right)^2 \right\rangle + s \left\langle \lambda \cdot \left(\nabla \hat{\mathbf{F}}^{T3} : \hat{\mathbf{B}} \right) \cdot \lambda \right\rangle + s \int_{\mathscr{A}_{\beta\sigma}} S_\Delta \frac{\mu_{ref}}{\mu} (\lambda \cdot \mathbf{A})^2 \, dA. \tag{C.4}$$

The tensor $\nabla \hat{\mathbf{F}}^{T3} : \hat{\mathbf{B}}$ represents the viscous dissipation of $\hat{\mathbf{F}}$ and is hence positive. The two other terms on the right-hand side of the above expression being also both positive, it results that $\hat{\mathbf{H}}_\mu$ is positive semi-definite.

References

[1] S.E. Spagnolie (Ed.), Complex Fluids in Biological Systems, Springer New York, 2015.

[2] F. Salehi, Rheological and physicochemical properties of vegetable juices and concentrates: A review, J. Food Process. Preserv. 45 (4) (2021).

[3] C. Fanelli, K. Kaouri, T.N. Phillips, T.G. Myers, F. Font, Magnetic nanodrug delivery in non-Newtonian blood flows, 2021.

[4] A. Skauge, N. Zamani, J.G. Jacobsen, B.S. Shiran, B. Al-Shakry, T. Skauge, Polymer flow in porous media: Relevance to enhanced oil recovery, Colloids Interfaces 2 (3) (2018) 27.

[5] Y. Peng, B.H. Lv, J.L. Yuan, H.B. Ji, L. Sun, C.C. Dong, Application and prospect of the non-Newtonian fluid in industrial field, Mater. Sci. Forum 770 (2013) 396–401.

[6] P. Saffman, G. Taylor, The penetration of a fluid into a porous medium or hele-shaw cell containing a more viscous liquid, Proc. R. Soc. Lond. Ser. A Math. Phys. Eng. Sci. (2016) 245312–245329.

[7] J. Hoyt, Some applications of non-Newtonian fluid flow, in: Rheology Series, Elsevier, 1999, pp. 797–826.

[8] S. Whitaker, The equations of motion in porous media, Chem. Eng. Sci. 21 (3) (1966) 291–300.

[9] C. Marle, Ecoulements monophasiques en milieu poreux, Rev. L'Inst. Français Pétrole XXII (1967) 1471–1509.

[10] S.P. Neuman, Theoretical derivation of Darcy's law, Acta Mech. 25 (3–4) (1977) 153–170.

[11] S. Whitaker, Flow in porous media I: A theoretical derivation of Darcy's law, Transp. Porous Media 1 (1) (1986) 3–25.

[12] J.-L. Auriault, Nonsaturated deformable porous media: Quasistatics, Transp. Porous Media 2 (1) (1987) 45–64.

[13] Y.-S. Wu, K. Pruess, Flow of non-Newtonian fluids in porous media, in: Advances in porous media, vol. 3, Elsevier, 1996, pp. 87–184, Chap. 2.

[14] R.P. Chhabra, J. Comiti, I. Machač, Flow of non-Newtonian fluids in fixed and fluidised beds, Chem. Eng. Sci. 56 (1) (2001) 1–27.

[15] T. Sochi, Non-Newtonian flow in porous media, Polymer 51 (22) (2010) 5007–5023, Publisher: Elsevier BV..

[16] T. Liu, S. Zhang, M. Wang, Does rheology of Bingham fluid influence upscaling of flow through tight porous media?, Energies 14 (3) (2021) 680.

[17] I. Battiato, P.T. Ferrero, D. O'Malley, C.T. Miller, P.S. Takhar, F.J. Valdés-Parada, B.D. Wood, Theory and applications of macroscale models in porous media, Transp. Porous Media 130 (1) (2019) 5–76.

[18] M.T. Balhoff, K.E. Thompson, A macroscopic model for shear-thinning flow in packed beds based on network modeling, Chem. Eng. Sci. 61 (2) (2006) 698–719.

[19] T. Shende, V. Niasar, M. Babaei, Upscaling non-Newtonian rheological fluid properties from pore-scale to Darcy's scale, Chem. Eng. Sci. 239 (2021) 116638.

[20] X. Lopez, P.H. Valvatne, M. Blunt, Predictive network modeling of single-phase non-Newtonian flow in porous media, J. Colloid Interface Sci. 264 (2003) 256–265.

[21] H.E. Fayed, N.A. Sheikh, O. Iliev, On laminar flow of non-Newtonian fluids in porous media, Transp. Porous Media 111 (1) (2015) 253–264.

[22] C.A. Bowers, C.T. Miller, Generalized Newtonian fluid flow in porous media, Phys. Rev. Fluids 6 (12) (2021) 123302.

[23] J. Lions, E. Sánchez-Palencia, Écoulement d'un fluide viscoplastique de Bingham dans un milieu poreux, J. Math. Appl. 60 (1981) 341–360.

[24] A. Bourgeat, A. Mikelić, A note on homogenization of Bingham flow through a porous medium, J. Math. Appl. IX Ser. 72 (4) (1993) 405–414.

[25] A. Bourgeat, A. Mikelić, Homogenization of a polymer flow through a porous medium, Nonlinear Anal. TMA 26 (7) (1996) 1221–1253.

[26] A. Bourgeat, S. Marušić, E. Marušić-Paloka, Écoulement non newtonien à travers un filtre mince, C. R. Acad. Sci.- Ser. I - Mathematics.

[27] J.-L. Auriault, P. Royer, C. Geindreau, Filtration law for power-law fluids in anisotropic porous media, Internat. J. Engrg. Sci. 40 (10) (2002) 1151–1163.

[28] A. Bourgeat, O. Gipouloux, E. Marušić-Paloka, Filtration law for polymer flow through porous media, Multiscale Model. Simul. 1 (3) (2003) 432–457.

[29] Z. Idris, L. Orgéas, C. Geindreau, J.-F. Bloch, J.-L. Auriault, Microstructural effects on the flow law of power-law fluids through fibrous media, Modelling Simulation Mater. Sci. Eng. 12 (5) (2004) 995–1015.

[30] T. Götz, H.A. Parhusip, On an asymptotic expansion for Carreau fluids in porous media, J. Eng. Math. 51 (4) (2005) 351–365.

[31] L. Orgéas, Z. Idris, C. Geindreau, J.-F. Bloch, J.-L. Auriault, Modelling the flow of power-law fluids through anisotropic porous media at low-pore Reynolds number, Chem. Eng. Sci. 61 (14) (2006) 4490–4502.

[32] L. Orgéas, C. Geindreau, J.-L. Auriault, J.-F. Bloch, Upscaling the flow of generalised Newtonian fluids through anisotropic porous media, J. Non-Newton. Fluid Mech. 145 (1) (2007) 15–29.

[33] T. Fratrović, E. Marušić-Paloka, Low-volume-fraction limit for polymer fluids, J. Math. Anal. Appl. 373 (2) (2011) 399–409.

[34] M. Anguiano, On the non-stationary non-Newtonian flow through a thin porous medium, ZAMM - J. Appl. Math. Mech. Z. Angew. Math. Mech. 97 (8) (2017) 895–915.

[35] M. Anguiano, F.J. Suárez-Grau, Homogenization of an incompressible non-Newtonian flow through a thin porous medium, Z. Angew. Math. Phys. 68 (2) (2017).

[36] M. Anguiano, Homogenization of a non-stationary non-Newtonian flow in a porous medium containing a thin fissure, European J. Appl. Math. 30 (2) (2018) 248–277.

[37] M. Anguiano, F.J. Suárez-Grau, Analysis of the effects of a fissure for a non-Newtonian fluid flow in a porous medium, Commun. Math. Sci. 16 (1) (2018) 273–292.

[38] C. Airiau, A. Bottaro, Flow of shear-thinning fluids through porous media, Adv. Water Resour. 143 (2020) 103658.

[39] S. Liu, J.H. Masliyah, On non-Newtonian fluid flow in ducts and porous media, Chem. Eng. Sci. 53 (6) (1998) 1175–1201.

[40] C.D. Tsakiroglou, A methodology for the derivation of non-Darcian models for the flow of generalized Newtonian fluids in porous media, J. Non-Newton. Fluid Mech. 105 (2–3) (2002) 79–110.

[41] X.-H. Wang, J.-T. Jia, Z.-F. Liu, L.-D. Jin, Derivation of the Darcy-scale filtration equation for power-law fluids with the volume averaging method, J. Porous Media 17 (8) (2014) 741–750.

[42] F. Zami-Pierre, R. de Loubens, M. Quintard, Y. Davit, Effect of disorder in the pore-scale structure on the flow of shear-thinning fluids through porous media, J. Non-Newton. Fluid Mech. 261 (2018) 99–110.
[43] A. Mikelić, An introduction to the homogenization modeling of non-Newtonian and electrokinetic flows in porous media, in: Lecture Notes in Mathematics, Springer International Publishing, 2018, pp. 171–227.
[44] O. Gipouloux, A.-M. Zine, Computation of the filtration laws through porous media for a non-Newtonian fluid obeying the power law, Comput. Geosci. 1 (2) (1997) 127–153.
[45] Y.I. Dimitrienko, L. Shuguang, Modeling of non-Newtonian fluid flows in porous textile structures under RTM technologies, J. Phys. Conf. Ser. 1990 (1) (2021) 012053.
[46] S. Li, Y. Dimitrienko, Mathematical modeling for the local flow of a generalized Newtonian fluid in 3D porous media, Appl. Math. Model. 105 (2022) 551–565.
[47] A. Bottaro, Flow over natural or engineered surfaces: an adjoint homogenization perspective, J. Fluid Mech. 877 (2019) 1–91.
[48] S. Whitaker, The Method of Volume Averaging, Springer Netherlands, 1999.
[49] H. Pascal, F. Pascal, Flow of non-Newtonian fluid through porous media, Internat. J. Engrg. Sci. 23 (1985) 571–585.
[50] J.R.A. Pearson, P.M.J. Tardy, Models for flow of non-Newtonian and complex fluids through porous media, J. Non-Newton. Fluid Mech. 102 (2002) 447–473.
[51] D. Lasseux, F.J. Valdés-Parada, F. Bellet, Macroscopic model for unsteady flow in porous media, J. Fluid Mech. 862 (2019) 283–311.
[52] D. Lasseux, F.J. Valdés-Parada, A. Bottaro, Upscaled model for unsteady slip flow in porous media, J. Fluid Mech. 923 (2021).
[53] J.-L. Auriault, C. Boutin, C. Geindreau, Homogenization of Coupled Phenomena in Heterogenous Media, ISTE & Wiley, 2009.
[54] J.C. Slattery, Advanced Transport Phenomena (Cambridge Series in Chemical Engineering), Cambridge University Press, 1999.
[55] S. Pasquier, M. Quintard, Y. Davit, Modeling flow in porous media with rough surfaces: Effective slip boundary conditions and application to structured packings, Chem. Eng. Sci. 165 (2017) 131–146.
[56] G.A. Zampogna, J. Magnaudet, A. Bottaro, Generalized slip condition over rough surfaces, J. Fluid Mech. 858 (2018) 407–436.
[57] U. Lācis, Y. Sudhakar, S. Pasche, S. Bagheri, Transfer of mass and momentum at rough and porous surfaces, J. Fluid Mech. 884 (2020).
[58] A. Bottaro, S.B. Naqvi, Effective boundary conditions at a rough wall: a high-order homogenization approach, Meccanica 55 (9) (2020) 1781–1800.
[59] L. Ferrás, J. Nóbrega, F. Pinho, Analytical solutions for Newtonian and inelastic non-Newtonian flows with wall slip, J. Non-Newton. Fluid Mech. 175-176 (2012) 76–88.
[60] O. Švec, J. Skoček, Simple Navier's slip boundary condition for the non-Newtonian lattice Boltzmann fluid dynamics solver, J. Non-Newton. Fluid Mech. 199 (2013) 61–69.
[61] E. Lauga, M. Brenner, H. Stone, Microfluidics: The No-Slip Boundary Condition, Springer Berlin, Heidelberg, 2007, pp. 1219–1240.
[62] F.A. Howes, S. Whitaker, The spatial averaging theorem revisited, Chem. Eng. Sci. 40 (8) (1985) 1387–1392.
[63] W.G. Gray, A derivation of the equations for multi-phase transport, Chem. Eng. Sci. 30 (2) (1975) 229–233.
[64] D. Lasseux, F.J.V. Parada, M.L. Porter, An improved macroscale model for gas slip flow in porous media, J. Fluid Mech. 805 (2016) 118–146.
[65] M. Agnaou, D. Lasseux, A. Ahmadi, From steady to unsteady laminar flow in model porous structures: an investigation of the first Hopf bifurcation, Comput. & Fluids 136 (2016) 67–82.
[66] D. Lasseux, F.J. Valdés-Parada, Symmetry properties of macroscopic transport coefficients in porous media, Phys. Fluids 29 (4) (2017) 043303.
[67] R.B. Bird, R.C. Armstrong, O. Hassager, Dynamics of polymeric liquids, in: Fluid Mechanics, vol. 1, second edition, John Wiley & Sons, 1987.
[68] R.I. Tanner, Engineering Rheology, second ed., Oxford University Press, Oxford, UK, 2000.
[69] D. Lasseux, A.A.A. Arani, A. Ahmadi, On the stationary macroscopic inertial effects for one phase flow in ordered and disordered porous media, Phys. Fluids 23 (7) (2011) 073103.
[70] D. Lasseux, F.J. Valdés-Parada, J.-F. Thovert, V. Mourzenko, Exuding porous media: deviations from Darcy's law, J. Fluid Mech. 911 (2021).